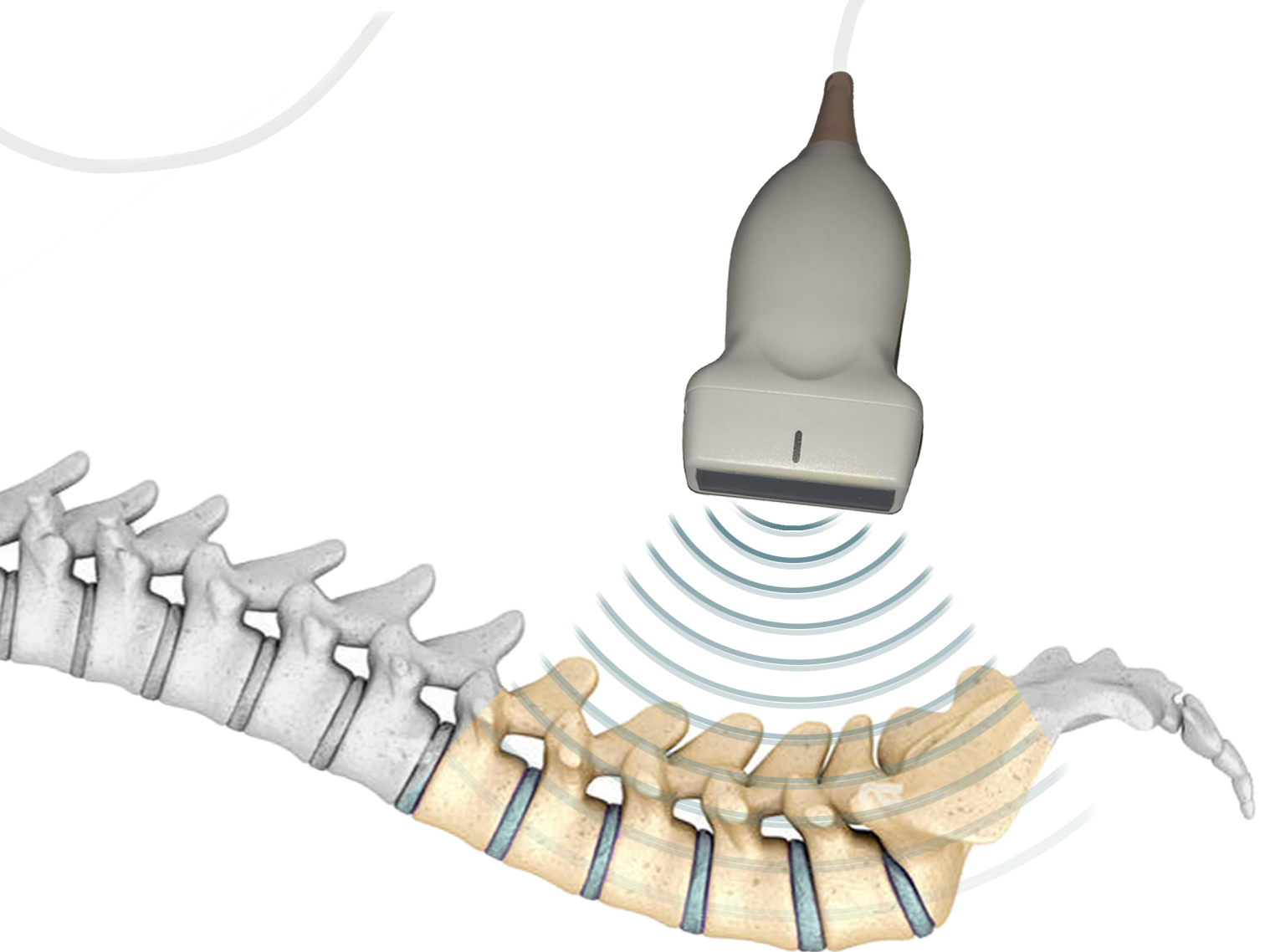# Level Localisation for Lumbar Surgery using Ultrasound

Technical Medicine
MSc thesis by Judith Sluijter

Level Localisation for Lumbar Surgery using Ultrasound

by

Judith H. Sluijter

Student number: 4453948

7th December, 2022

Thesis in partial fulfilment of the requirements for the joint degree of Master of Science in

Technical Medicine

Leiden University | Delft University of Technology | Erasmus University Rotterdam

Master thesis project (TM30004, 35 ECTS)
Erasmus MC
Department of Neurosurgery and Radiology & Nuclear Medicine
March 2022 - December 2022

Chair and medical supervisor:	Prof. Sieger Leenstra	Erasmus MC
Technical supervisor:	Dr. Theo van Walsum	Erasmus MC
Independent committee member:	Dr. Frans Vos	TU Delft

An electronic version of this thesis is available at `http://repository.tudelft.nl/`.

Preface

With this graduation project, my seven years of studying at the TU Delft, Erasmus University and Leiden University are ending. In 2015, Clinical Technology seemed the right fit, a study to explore and develop my interest in technological innovations and healthcare. Now, I can finally tell you - it definitely was the right choice!

During my internships, I became increasingly interested in image-guided surgery. The use of advanced imaging techniques to improve surgery fascinates me because of its innovative character and direct impact on the patient's health. This graduation project immediately stood out when I talked to Theo about potential graduation projects. It contained all my wishes: a direct connection to the clinical practice, an interesting department for my clinical exposure, enthusiastic supervisors and a challenging topic, as I had never worked with ultrasound and deep learning. Now, nine months later, I learned a lot about performing a clinical study, ultrasound acquisition, deep learning, and neurosurgery, and I developed myself personally. Conducting two projects in my Master's thesis was challenging, but I am proud of the result and all I have learned during this thesis. I truly enjoyed working on this project and look back to it as an exciting and challenging experience. I am excited to stay in the Erasmus MC to combine my medical and technical knowledge as a Technical Physician in the Radiotherapy department.

I would like to thank my supervisors, Sieger and Theo, for their valuable insights, critical eye, and motivating attitude. Sieger, your enthusiasm for this project worked contagious on me. I enjoyed our discussions on technological innovations in medicine between the surgeries in the Maasstad. Theo, thank you for your insights and for helping me to take my research to a higher level. Although you supervise many PhD and master students, you always managed to take time for me whenever I had questions. Furthermore, I would like to thank the involved neurosurgeons, Erik and Jochem. They welcomed me kindly during their ORs and gave valuable input from a neurosurgeon's point of view. Also, thanks to the anesthesiologists and OR staff in the Maasstad hospital for their willingness to help me and their interest in my project. Lastly, thanks to all the students of the BIGR group for our discussions on the 26th floor. Furthermore, I would like to thank the patients who participated: without them, this project would not be possible.

And most of all, I want to express my gratitude to my parents, sister, Sjoerd, roommates Julia and Marleen, and friends. They always listened to my stories and helped me put things in perspective. Thanks for the unconditional support and belief in me and for making my student time unforgettable.

Judith Sluijter
Rotterdam, December 2022

List of Abbreviations

AR	Augmented reality
BMI	Body mass index
CI	Confidence interval
CT	Computed tomography
EHR	Electronic health record
FOV	Field of view
GEHC	GE HealthCare
IGS	Image-guided surgery
IRB	Institutional Review Board
LSS	Lumbar spinal stenosis
MRI	Magnetic resonance imaging
OR	Operating room
PET	Positron emission tomography
ROI	Region of interest
SP	Spinous process
TGC	Time gain compensation
US	Ultrasound
WLS	Wrong-level surgery

Summary

Wrong-level spine surgery (WLS) is a medical error with severe consequences for the patient and medical staff. The current golden standard to prevent WLS during spinal surgery is fluoroscopy images acquired by a C-arm. However, this approach uses ionising radiation and interrupts the standard surgical workflow. To overcome these disadvantages, ultrasound-based navigation may provide an alternative to prevent WLS during spinal surgery. Baka et al. developed the Lumbar Localiser for ultrasound-based level localisation; however, this has not yet been applied in clinical practice. This project aims to improve and evaluate this level localisation approach in clinical practice.

Chapter 1 highlights the social relevance of ultrasound-based level localisation.

Chapter 2 shows in a literature review that navigated ultrasound-based guidance is not yet implemented in clinical practice. Identified recommendations for further research were optimising ease of use, workflow integration, registration accuracy and computation time.

Chapter 3 describes a prospective multi-centre study (n=34) which evaluated the accuracy of the level localisation approach and the added value of intraoperative ultrasound acquisition. The accuracy of the improved level localisation approach was too low (53%) to recommend implementation in clinical practice. We showed that pre- and intraoperative ultrasound acquisitions could be integrated efficiently into the operation room (OR) workflow, with clinically negligible time differences compared to the current approach for level localisation. Intraoperative ultrasound acquisition added valuable information, enabling a re-check of the level localisation without the attenuating subcutaneous fat layer between the SP and ultrasound transducer.

Chapter 4 describes the development of an automated contour segmentation approach based on magnetic resonance imaging (MRI) using deep learning. A nnU-Net was trained to segment the lumbar spinous process automatically. Subsequently, the posterior contours were extracted based on these segmentations and imported into the Lumbar Localiser. The automatic contours showed a successful matching in all 16 test cases.

Chapter 5 provides an overall conclusion and discussion.

In this master's thesis, the technical aspects and clinical workflow of the Lumbar Localiser were improved to get closer to the clinical application of ultrasound-based level localisation for lumbar surgery. Implemented improvements include adding intraoperative ultrasound acquisition, extension to MRI as a preoperative modality and automatisation of the contour annotation. In conclusion, this approach cannot be applied yet in clinical practice, as an accuracy of around 100% should be achieved to minimise the risk of WLS and thereby prevent irreversible damage to the patient.

Contents

1

General introduction and thesis outline

Current times ask for a transition of the healthcare system. As the Dutch government stated in the 'Green Deal Duurzame Zorg', the health of patients and healthcare workers should be promoted by ensuring an optimal working environment [1]. The health of patients and healthcare workers is threatened by increasing staff shortages, causing delayed medical care and high working pressure. This shortage is estimated at 117.000 healthcare workers in 2030 [2]. Optimal working conditions should be ensured to maintain current and attract new healthcare workers. One way to ensure an optimal working environment is to reduce the health risks for patients and healthcare workers in medical procedures. A safer working environment can be promoted by minimising the use of ionising radiation. Radiation can cause alterations within our body cells, which may cause eventual harm, such as cancer. Therefore, every application that uses ionising radiation should be evaluated regularly to determine whether the benefits outweigh the risks. The use of radiation and radioactive substances increases over time as it has more than doubled over the last two decades [3]. Therefore, we should evaluate if new technologies or new applications of current technologies can replace existing radiation applications.

In this master's thesis, we focus on spinal surgery. It is crucial to perform spinal surgery on the correct level. Wrong-level spine surgery (WLS) is a medical error which has severe consequences, demanding re-surgery, affecting the patient's health and impacting the surgeon's and the team's confidence [4], [5]. The current golden standard for level localisation is fluoroscopy images acquired by a C-arm. Still, WLS occurs occasionally, reporting incidences of 0.1% to 3.3% [6]–[8]. Fluoroscopy images are sometimes hard to interpret, especially in obese or older patients with lower bone density. Besides, fluoroscopy uses ionising radiation, exposing patients and healthcare workers to radiation. Ultrasound-based navigation is a safe alternative, as it can potentially prevent WLS without using ionising radiation. Baka et al. proposed an ultrasound-based level localisation approach for spinal surgery [9].

This project aims to improve the current ultrasound-based level localisation approach, with the ultimate goal of implementing it in clinical practice, replacing the C-arm. The following subgoals were set for this project:

1. Conduct a literature review to overview the history and current applications of ultrasound-based guidance in neurosurgery to highlight future opportunities.
2. Perform a clinical study to evaluate the overall accuracy of the level localisation technique, improve the workflow in the operating room (OR) and assess the added value of intraoperative ultrasound acquisition.
3. Automate contour extraction of preoperative images to improve user-friendliness and reduce user-variability of the ultrasound-based level localisation approach.

This thesis is composed of five chapters.

Chapter 1, this chapter highlights the social relevance and states the outline of the thesis.

Chapter 2 provides a literature review of the history and current applications of stand-alone and navigation-based ultrasound guidance for spinal and cranial neurosurgery. Differences between these applications are described and future opportunities are highlighted.

Chapter 3 describes the results of a clinical study on level localisation for lumbar surgery using ultrasound. The accuracy of the pre- and intraoperative ultrasound-based level localisation is presented. Furthermore, the improved workflow and approach are described and recommendations for further improvements are highlighted.

Chapter 4 presents an automatic approach to extract the contours of the spinous process based on MRI using deep learning. The results are evaluated on an internal and an external data set.

Chapter 5 provides an overall discussion and conclusion. Lastly, the most important future challenges and research recommendations are discussed.

2

Ultrasound-based guidance in neurosurgery: a review

Judith H. Sluijter, BSc
Erasmus MC, Rotterdam, the Netherlands
Department of Neurosurgery and Radiology & Nuclear Medicine
30th June 2022

2.1. Introduction

Precise identification of the anatomy in neurosurgery is essential given the proximity of critical functional areas and vascular structures in the brain and around the spine [10]. Image-guided surgery (IGS) assists the neurosurgeon in accurately visualising the anatomy and localising target tissue during a procedure [11]. IGS is any procedure that uses images during surgery. Over the last decades, imaging technologies have significantly developed, resulting in many imaging modalities being applied in clinical practice. Imaging modalities for IGS include X-ray, ultrasound, computed tomography (CT), magnetic resonance imaging (MRI) and fluorescence imaging. Nuclear images are also used, for example, positron emission tomography (PET) and radioactive tracers. The broad concept of IGS includes many applications, from low-end solutions such as X-ray to remove a foreign object from inside the body to high-end solutions such as fluorescent-labelled isotopes to identify tumour tissue during surgery.

A subset of IGS is navigation, which uses a real-time spatial correlation of preoperative images or planning onto the patient. In navigation, the position of a surgical instrument is visualised in relation to the surrounding anatomic structures of the patient [12]. Nowadays, navigation is a standard procedure in neurosurgery, serving multiple purposes: entry point determination, pathway guidance, and lesion localisation. The first purpose, entry point determination, uses tracked instruments to determine the incision location or the biopsy insertion point. Subsequently, pathway guidance is applied after the incision to follow a preoperatively planned trajectory using tracked devices. Following this predefined path, the navigation guides the surgeon to the target during surgery, minimising potential damage to crucial structures. For example, in pedicle screw placement, the pathway of the screws can be tracked during spinal fusion surgery to reduce the rate of screw misplacement [13]. The third navigation purpose is lesion localisation to precisely identify the position of the target tissue, which is essential to differentiate between the lesion and the surrounding tissue. Pathway guidance and lesion localisation can be challenging tasks due to tissue deformation, which occurs after incision.

Navigation systems use both preoperative and intraoperative images. Commonly used preoperative images in neuronavigation are CT and MRI. Registration is a crucial navigation component as it obtains alignment of these preoperative images to the patient's intraoperative anatomy [16]. This registration,

Figure 2.1: Evolution of ultrasound technology. Left: transverse ultrasound scan of the cervical spine acquired by Reid et al. in 1978 [14]; middle: current quality of ultrasound images, also a transverse scan of the cervical spine [15]; right: colour Doppler ultrasound of the same anatomical area [15].

specifically medical image registration, can be classified into two categories: 1) object-based methods, based on foreign objects introduced in the image space, and 2) anatomy-based methods, based on the patient's image information [17]. Object-based registration uses invasive markers such as a stereotactic frame or non-invasive markers such as skin patches to align the images to the patient. Anatomy-based methods generally use intraoperative images and rely on points, landmarks, surfaces, or image intensities. Commonly used intraoperative images are X-ray and ultrasound. A disadvantage of intraoperative X-ray is ionising radiation, exposing the patient, surgeon and operation room (OR) staff to radiation. Moreover, the use of X-ray results in interruption of the standard surgical workflow as the OR staff must position the X-ray system around the sterile field. Furthermore, the surgeon and OR staff must wear lead skirts or stand behind a radiation shielding screen. Intraoperative ultrasound overcomes these disadvantages since no ionising radiation is used, and easy to incorporate into the standard surgical workflow.

Despite these advantages of intraoperative ultrasound, its widespread use in neurosurgery, especially spinal surgery, remains limited. This review aims to overview the history and current applications of ultrasound-based guidance in neurosurgery to highlight future opportunities. The first part of this review outlines the stand-alone use of ultrasound in neurosurgery. The second part focuses on ultrasound-based navigation in neurosurgery.

2.2. Stand-alone ultrasound guidance

2.2.1. History
The evolution of intraoperative ultrasound started around the 1960s when researchers introduced non-real-time ultrasound to the clinic [18]. Ultrasound was then applied to localise lesions during cranial surgery [18]. Initially, ultrasound was not widely accepted because non-real-time images were hard to interpret. This changed when real-time ultrasound became available by improving ultrasound technology and instrumentation during the late-1970s [18], [19]. The first clinical case of the use of real-time ultrasound during neurosurgical procedures was in the spine, described in 1978 by Reid et al., in which focused and narrow beam ultrasound systems were used to visualise a cystic lesion in the cervical spine (Figure 2.1) [14]. After introducing ultrasound imaging of the spinal cord, cerebral ultrasound applications were applied in 1981 [20]. Dohrmann and Rubin used ultrasound to visualise intracranial structures before opening the dura mater [21]. Subsequently, this imaging modality proved its value in spinal and cranial surgery for tumours, cysts, and disc hernias [18]. The ultrasound images enabled step-by-step procedure guidance, as multiple images can be acquired during surgery [22]. However, low-resolution images, difficulty in image interpretation and orientation, lack of specific knowledge and training, and often use of low-end ultrasound systems limited the widespread use of the ultrasound [23]. Around 1990, the introduction of colour Doppler imaging and laparoscopic ultrasound resulted in substantial improvements in ultrasound techniques (Figure 2.1) [18]. With advancements in spatial and temporal resolution, these developments resulted in a growing scientific and clinical interest in ultrasound use in neurosurgery [24].
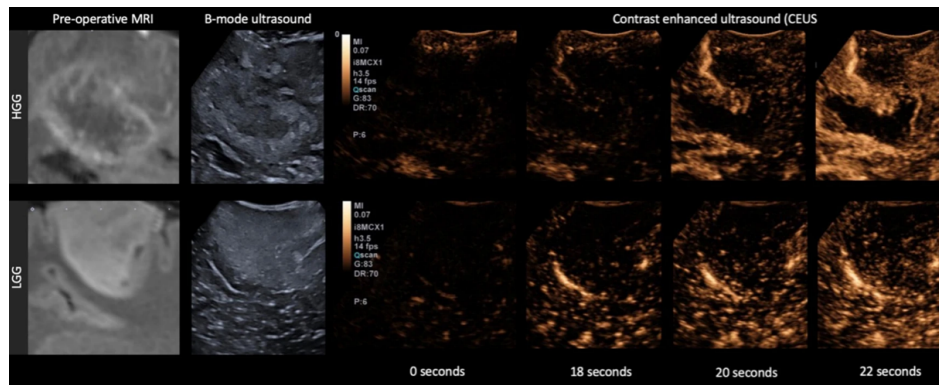
Figure 2.2: Contrast-enhanced ultrasound using intravenously injected gas-filled microbubbles can differentiate between a high-grade (top row) and low-grade (bottom row) glioma [29].

2.2.2. Cranial surgery

Ultrasound during cranial surgery is only applied after craniotomy because the skull blocks the transmission of ultrasound waves. Nowadays, stand-alone ultrasound is used to help the surgeon confirm whether tumour tissue is reached [25]. Moreover, researchers have investigated the ability of ultrasound to distinguish between tumour and normal brain tissue [25]–[27]. These studies show that conventional intraoperative ultrasound often fails to discriminate tumours from normal tissue. On the other hand, advanced ultrasound techniques, such as contrast-enhanced ultrasound using intravenously injected gas-filled microbubbles, can successfully differentiate between these tissue types (Figure 2.2)[24], [28]. Another advanced modality is the use of molecular imaging in ultrasound. These molecular images can differentiate between benign and malignant brain tumours or low-grade and high-grade tumours [28]–[31].

2.2.3. Spinal surgery

The vertebrae limit the general application of ultrasound in spinal surgery, as sound waves cannot penetrate through bone (Figure 2.3). As a result, clinicians can use ultrasound to examine lesions posterior to the vertebrae. Clinicians can examine lesions in the spinal cord using ultrasound only after laminectomy. Nowadays, neurosurgeons use ultrasound to identify anatomy for various spinal diseases, for example, trauma, degenerative diseases, vascular diseases, and tumours [32]. A systematic review by Patel et al. concluded that ultrasound successfully identifies tumour tissue in spinal surgery [33]. They included seven oncologic studies with 1523 patients, and all included studies reported successful lesion identification using ultrasound. Besides tumour tissue, ultrasound is also helpful for guiding and evaluating spine decompression [34]. Moreover, other areas than neurosurgery have successfully adopted stand-alone ultrasound in spinal care, such as epidural and spinal anaesthesia [33].

Although neurosurgeons use ultrasound often during surgery, stand-alone use suffers from limitations such as the lack of orientation and panoramic view [23]. To overcome these limitations, ultrasound-based navigation was introduced, which uses intraoperative ultrasound to register preoperative CT or MRI to the patient.

2.3. Ultrasound-based navigation

2.3.1. History

To understand the history of ultrasound-based navigation in neurosurgery, we first describe the history of navigation in neurosurgery. Originally, navigation was primarily applied in cranial surgery, using stereotactic head frames [11], [36]. Stereotactic head frames are attached to the patient's skull to provide reference points for precise localisation of intracranial targets. These frames use a three-dimensional (3D) coordinate system with preoperative information about the patient's anatomy [37]. Horsley and Clarke described the first use of these frames in 1908 to accurately direct a surgical transducer to a predefined target in a monkey's brain [38]. Spiegel and Wycis described the first-in-human use of a stereotactic frame to localise intracranial structures in 1946 [39]. The introduction of CT imaging in the 1970s increased interest in navigation, as surgeons could now visualise their targets using

Figure 2.3: Acoustic shadow posterior to the spinous process in spinal ultrasound scanning as the sound waves cannot penetrate through bone.
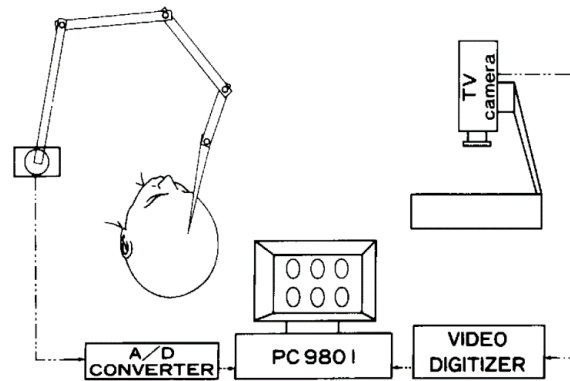

Figure 2.4: Block diagram of the frameless system proposed by Watanabe et al. [35]. They connected a multi-joint, three-dimensional position sensor to the microcomputer. Preoperative images are sampled through TV camera by video digitising system.

3D preoperative images [11]. Watanabe et al. described the first frameless neuro-navigation system in 1987, removing the inconvenient and surgical working space limiting frame [35]. They used a 3D sensing arm which could determine the 3D coordinates of the sensor tip of the arm derived from the angles of the joints and the lengths of the separate segments (Figure 2.4). Subsequently, the positions of three anatomical landmarks are fed into the computer by placing the sensor tip at each landmark. These three landmarks were annotated on preoperative CT images using small metal markers. A positional relationship between the CT images and the patient's head could be calculated using the corresponding points. Subsequently, this relationship was used to translate the real-time position of the sensor tip into the CT axis and to display this position with a cursor on the corresponding plane of CT images.

After its introduction, frameless approaches evolved by combining IGS with MRI as preoperative images. The success of the frameless approaches promoted further development of image-based registration methods. Wirtz et al. reported a successful image-based registration method based on intraoperative MRI in 1997 [40]. Their intraoperative images updated the preoperative data set with the potentially shifted intraoperative anatomy of the patient. In 1998, Comeau et al. presented a surgical guidance system that combined preoperative MRI and CT images with intraoperative ultrasound images to detect brain tissue deformation during cranial surgery [41]. It was in the early 1990s that navigation applications for spine interventions were introduced. These initial efforts relied on navigation technologies initially developed for cranial procedures [42].

Ultrasound-based navigation in neurosurgery was introduced in 1994 by Trobaugh et al. [43]. They tracked the spatial position of the ultrasound transducer during cranial surgery. Subsequently, the preoperative images were reformatted to correspond to the orientation of the ultrasound images. These reformatted and ultrasound images were displayed next to each other, allowing surgeons to understand them better. Since then, ultrasound-based navigation has been gradually introduced in neurosurgery.

2.3.2. Cranial surgery

Since the last decade, neurosurgeons have applied ultrasound-based navigation during cranial surgery (Figure 2.5) [24]. During cranial surgery, discrepancies occur between the preoperative scans and the current intraoperative situation, as brain shift occurs after craniotomy and tumour resection. Researchers proposed different registration methods based either on a tracked transducer or the related anatomy between the images. Ohue et al. and Wu et al. used a tracked transducer to provide information on the spatial position and orientation of the ultrasound images [44], [45]. A similar method was used by Thorough et al., matching orientations and displaying the ultrasound and preoperative images next to each other [43]. Prada et al. used a similar method, using a tracked transducer to calculate the orientation of the transducer to the anatomy of the patient [46]. They created a merged view between ultrasound and MRI (Figure 2.6).
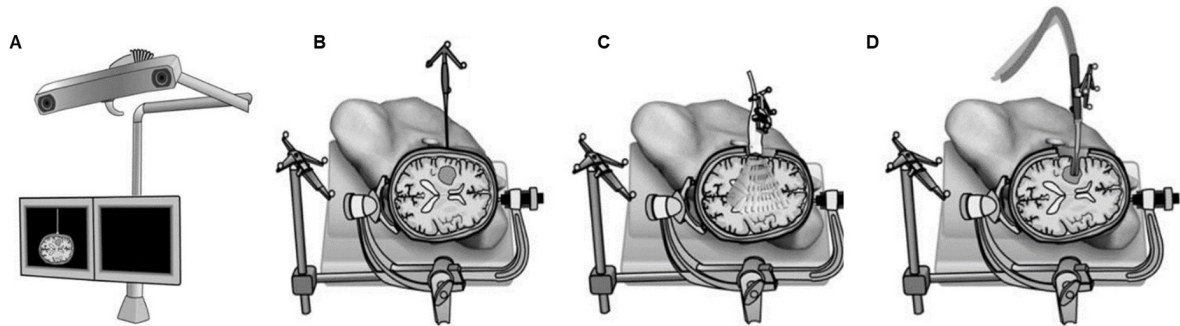
Figure 2.5: Ultrasound-based navigation system for cranial surgery. A) An optical camera system tracks all surgical instruments, and the navigation monitor displays the overlay on preoperative images; B) Navigated preoperative planning during surgery using a tracked pointer; C) Freehand 3D ultrasound acquisition after incision using a tracked ultrasound transducer; D) Navigated resection using a tracked device [48].
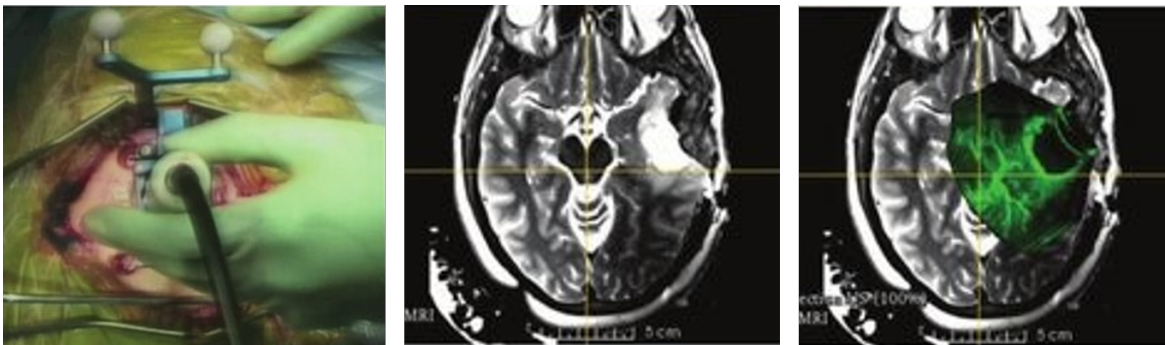

Figure 2.6: Intraoperative ultrasound in cranial surgery. Left: intraoperative 2D ultrasound during tumour resection. Middle: intraoperative MRI after initial tumour resection. Right: registered image of intraoperative 3D ultrasound and intraoperative MRI [49].

Another study by Nitsch et al. segmented the falx cerebri and tentorium cerebelli in ultrasound and MRI [47]. These segmentations served as guiding frames for intensity-based image registration. The mean target registration error (TRE) was 3.8 millimetres (mm) for the registration without segmentations and 2.2 mm for the combined segmentation and registration approach. The computation time for the first registration was 40.5 seconds, which was reduced to 12.0 seconds by including the segmentations.

2.3.3. Spinal surgery

In contrast to cranial surgery, ultrasound-based spine navigation is not yet introduced in the clinic, although researchers have investigated this topic [50], [51]. A systematic review by Gueziri et al. in 2020 included 53 articles which reported on ultrasound-based spine navigation [52]. Most of the included articles used tracked ultrasound to register preoperative CT or MRI to the patient. Most authors evaluated this on phantoms, human cadavers or animal cadavers. They proposed different methods for registration, such as mapping the preoperative CT images to simulate ultrasound-like images to register the tracked ultrasound images to these mapped CT images [53]. Gueziri et al. based their initial alignment of CT to ultrasound on the ultrasound scan trajectory [54]. They refined this initial transform by matching the locations of the posterior vertebra surface on both images (Figure 2.7). A median TRE of 1.48 mm was demonstrated within 11 seconds of computation time, thereby meeting their requirements in accuracy and computation time [54].

Clinical domains other than neurosurgery have also investigated ultrasound-based spinal navigation. For example, Nagpal et al. proposed using ultrasound to register preoperative CT to the patient to provide the clinician with anatomic images during spinal needle injections [55]. They globally aligned the lumbar spine between the CT and ultrasound data using intensity-based and point-based registration using set correspondences. Subsequently, they performed a multi-vertebrae registration step to account for possible curvature change of the spine between the supine CT and prone-position ultrasound
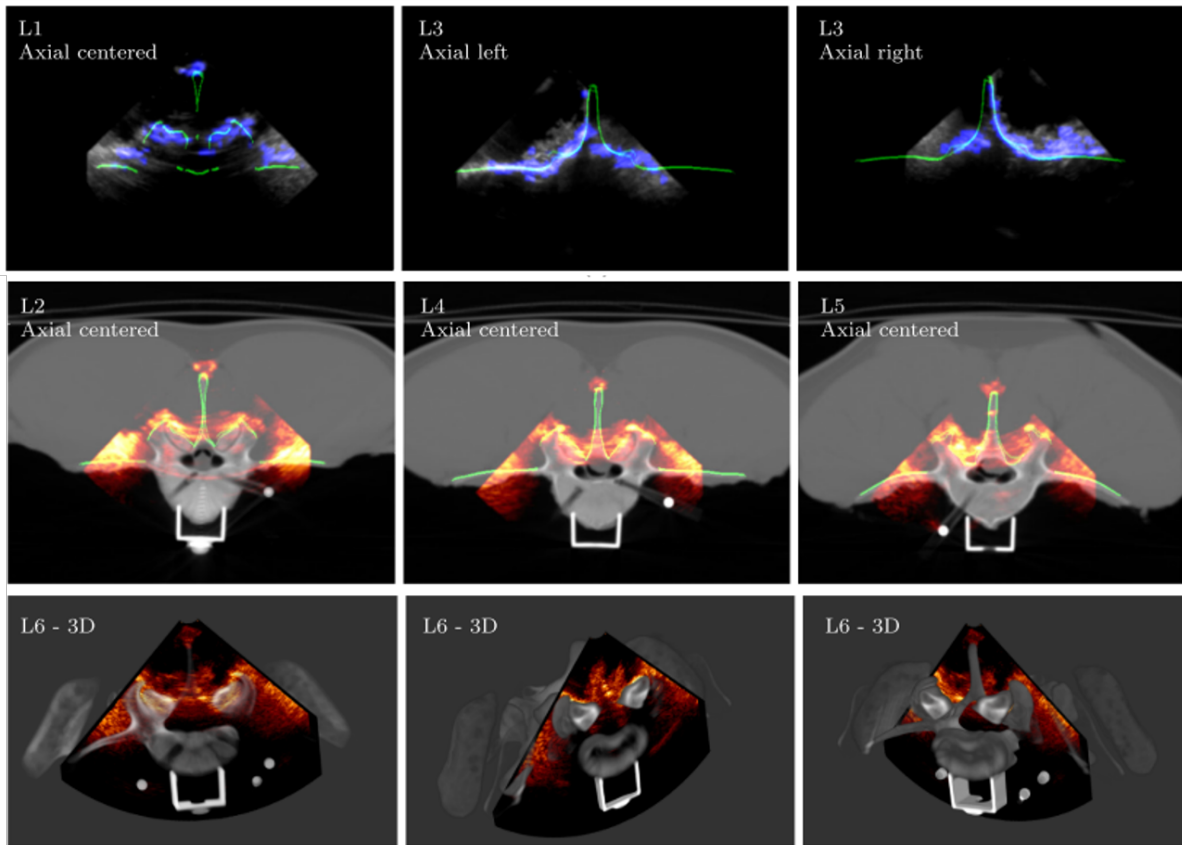
Figure 2.7: Qualitative registration results at various vertebral levels. Top row: Alignment of ultrasound image (grey), extracted posterior vertebra surface of the ultrasound image (blue), and CT scan (green). Middle row: Alignment of ultrasound image (heat map), CT image (grey), and CT extracted posterior surface of the vertebra (green). Bottom row: 3D views of ultrasound slice aligned with CT volume [54].

images. Introduced points constrained the movement of the individually transformed vertebrae to ensure the optimal alignment is physically possible. They evaluated their algorithm in ten clinical patient datasets and demonstrated a mean TRE of 1.37 mm with 50-185 seconds runtime. Several studies proposed solutions for segmenting these posterior vertebrae surfaces on ultrasound images. Most spinal surgeries are performed using a posterior approach, with the patient in the prone position. During this approach, only the posterior surface of the vertebrae is visible on the ultrasound scans because the bony vertebrae produce an acoustic shadow. Baka et al. proposed a deep convolutional neural network-based bone segmentation algorithm for ultrasound images [9]. They matched the segmented intraoperative ultrasound images to manually segmented preoperative X-ray images. They aimed to indicate the vertebrae levels using ultrasound to provide level localisation during hernia surgery. The final labelling was correct in 92% of the cases, demonstrating the feasibility of ultrasound-based surgical entry point detection for spinal surgeries. Chen et al. proposed another vertebrae segmentation approach, which used local phase filtering of the ultrasound volume with subsequent raycasting to remove any soft tissue visible above the bone signals [56].

2.4. Discussion

This review provided an overview of the history and current applications of ultrasound-based guidance in neurosurgery. Several gaps and discrepancies in the different applications of ultrasound-based guidance in neurosurgery were identified and will be described in this section. Moreover, future research opportunities in this field will be highlighted. Finally, the limitations of this study will be described.

2.4.1. Image-guided surgery, navigation and ultrasound

First, IGS, navigation and ultrasound are reflected in general. IGS has found its permanent introduction in surgery in all kinds of clinical domains. This development is rapidly incorporated into the surgical workflow, given that CT and MRI scans were not even introduced half a decade ago. Moreover, dedicated navigation systems are currently integrated into the standard surgical workflow of cranial neurosurgery. These systems use surface and landmark registration with tracked instruments to register preoperative CT and MRI to the patient. However, these systems are expensive as they cost around $500.000 [57]. Ultrasound-based navigation might be an alternative, as intraoperative ultrasound has significant benefits over other intraoperative navigation tools in terms of cost, easiness of use, and adaptability to multiple clinical scenarios [23]. For example, the conventional ultrasound system of the current institute costs $15.000 [58]. Moreover, they can easily be integrated into existing OR infrastructure with minimal disruption to the surgical workflow. On the other hand, intraoperative ultrasound is user-dependent with a steep learning curve. Neurosurgeons do not receive standard training in ultrasound use and image interpretation. Furthermore, ultrasound does not propagate past bony structures or pockets of gas. Therefore, cranial ultrasound can only be applied after craniotomy. Clinicians can only examine the spinal cord anatomy with ultrasound when laminectomy is performed. In addition, ultrasound systems are calibrated to assume a sonic transmission speed of 1540 ms^{-1}, the mean velocity of sound in soft tissue [16]. However, significant distortion of the ultrasound images may occur if tissues containing a different propagation velocity are scanned, such as fat (1475 ms^{-1}). This difference in propagation velocity might cause lower-quality images, primarily for preoperative spinal ultrasound scanning, because of the local subcutaneous fat layer posterior to the spine. Despite these challenges, ultrasound is considered a reliable tool for IGS and navigation. The use of ultrasound will likely increase further in the coming decade as the technology keeps improving with innovations such as contrast-enhanced imaging and molecular imaging. These innovations differentiate tumour tissue from normal tissue, thereby assisting in target delineation and resection control.

2.4.2. Discrepancies in ultrasound-based guidance

Several discrepancies are observed in the clinical application of ultrasound-based guidance in neurosurgery. First, the current clinical application of stand-alone ultrasound differs between cranial and spinal surgery. Reflecting on the history of stand-alone use of ultrasound, we observe that it was applied in spinal surgery before cranial neurosurgery. The opposite situation exists in the current clinical practice, as ultrasound is more extensively applied in cranial neurosurgery than spinal neurosurgery. Advanced ultrasound techniques, such as contrast-enhanced ultrasound using microbubbles, promoted the use of ultrasound for cranial surgery.

Second, ultrasound-based navigation also shows a discrepancy between cranial and spinal applications. While ultrasound-based navigation is applied in the OR for cranial surgery, it is not yet applied in a clinical setting for spinal surgery. The discrepancy between these applications is also observed in the history of navigation in neurosurgery. Navigation was initially developed for cranial surgery, using stereotactic head frames. The rigid skull creates a solid reference for navigation, whereas the vertebras are flexible structures. Spinal navigation was introduced approximately 40 years later than cranial navigation and relied on technologies that were initially developed for cranial procedures [42].

2.4.3. Recommendations for future research

Several factors contribute to the absence of ultrasound-based spine navigation, including the need for a standard methodology to assess the accuracy, robustness, reliability, and usability of the registration method [52]. Ultrasound-based spinal navigation could be introduced into clinical practice. Gueziri et al. concluded that, when successfully implemented, ultrasound-based spinal navigation has satisfactory accuracy, robustness and reliability [52]. More dedicated research on this topic should be performed,

optimising the workflow integration, registration accuracy and computation time. Neurosurgeons, engineers and researchers should closely collaborate in an interactive process to ensure a permanent application of this innovation. Moreover, legal regulations must be considered before this navigation tool can be applied to the clinic.

Moreover, future research should learn from acquired knowledge and practical experience of similar applications. For example, lessons can be learned from cranial applications, such as segmentation of anatomical structures on both images to improve the registration accuracy and decrease the calculation time, as Nitsch et al. showed [47]. Furthermore, knowledge can be acquired from using non-ultrasound-based navigation in spinal surgery, such as fluoroscopy-based pedicle screw placement. Also, the application of ultrasound-based spine navigation in other clinical domains should be considered, such as its use in spinal needle injections.

Innovations in ultrasound-based spinal navigation might accelerate this acceptance, for example, augmented reality (AR). AR allows the neurosurgeon to visualise the image guidance without looking away from the surgical field. Liu et al. concluded in a systematic review that AR guidance systems show high potential value in practical clinical applications for spinal surgery [59]. Currently, the most popular AR application in spine surgery is pedicle screw instrumentation. More research should be performed to accomplish the generic application of this technology to ultrasound-based navigation and other spinal applications.

2.4.4. Limitations
A limitation of the current review is the non-systematic literature search. As a result, relevant articles may be missed. However, this review did not aim to provide a complete overview but to present a comprehensive background of the broad concept of IGS in neurosurgery to highlight future opportunities. A systematic review should be performed to identify the current techniques proposed for spinal ultrasound-based navigation.

2.5. Conclusions
This literature review shows that stand-alone and navigated ultrasound-based guidance are used in cranial surgery, whereas only stand-alone ultrasound guidance is used in spinal surgery. We regard intraoperative ultrasound as a valuable tool in neurosurgery since it is radiation-free and easy to incorporate into the standard surgical workflow. Therefore, further research should be performed on ultrasound-based navigation in spinal surgery. They should aim to improve the registration accuracy, computation time, and ease of use on the OR. Further innovations may include introducing advanced ultrasound techniques for targeted-specific imaging and augmented reality.

3

Level localisation for lumbar surgery using ultrasound

3.1. Introduction

3.1.1. Lumbar surgery

Lumbar surgery refers to any surgery in the lumbar spine involving the L1-S1 vertebrae (Figure 3.1). Two common indications for lumbar surgery are lumbar spinal stenosis (LSS) and a herniated disc. LSS, first described by Verbiest in 1949, is characterised by the narrowing of the spinal canal and the nerve root canals, leading to compression of neural and vascular structures [60]–[62] (Figure 3.2). The most common symptom is neurogenic claudication, characterised by pain, cramping or heaviness in the lower back, legs or hips with standing or walking [63]. LSS is the most common reason for patients older than 65 to undergo spinal surgery [64]. Persistent complaints arising from LSS can be treated surgically with laminectomy, removing the lamina and spinous process (SP) to decompress the nerve roots (Figure 3.2).

A lumbar herniated disc occurs when the nucleus pulposus or annulus fibrosis displace beyond the intervertebral disc space, thereby causing radiculopathy (Figure 3.3). The highest prevalence is among people aged 30 to 50, with a male-to-female ratio of 2:1 [65]. A spinal hernia can be surgically treated with a discectomy, removing the intervertebral disc (Figure 3.3).
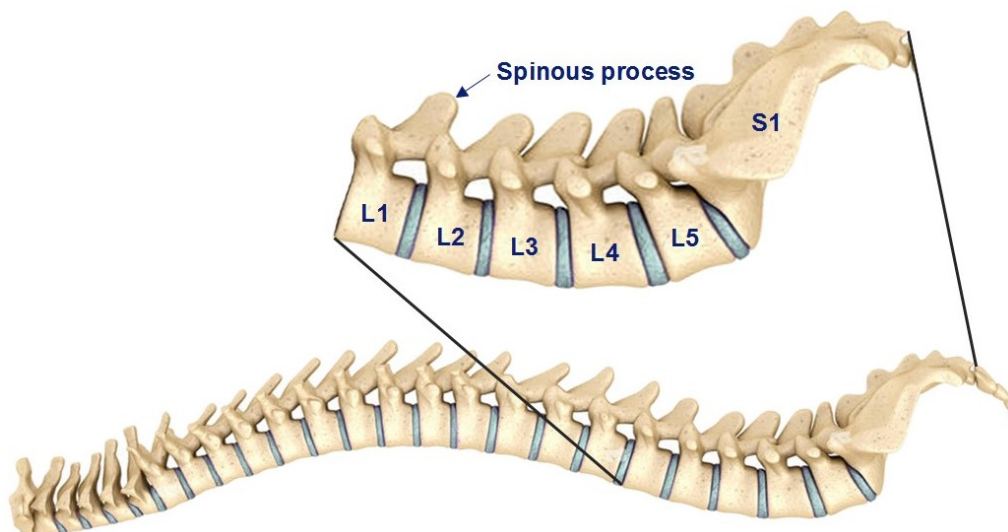

Figure 3.1: Schematic overview of the spine anatomy, with a highlighted lumbar spine. L1-L5: lumbar vertebrae 1-5; S1: sacrum [66].
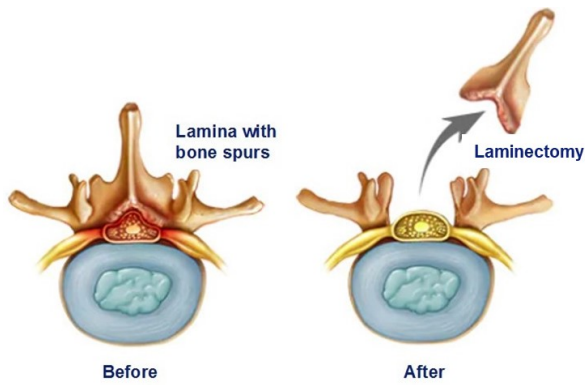
Figure 3.2: Schematic overview of a laminectomy to surgically treat spinal stenosis [67].
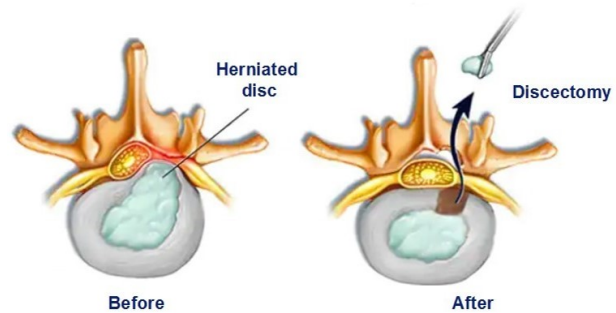
Figure 3.3: Schematic overview of a discectomy to surgically treat a herniated intervertebral disc [68].

3.1.2. Level localisation

It is crucial to perform lumbar spinal surgery on the correct level. LSS and a herniated disc are evidently visible on preoperative magnetic resonance imaging (MRI). However, it is difficult to identify the level of surgery on the patient's body in the operating room (OR). Wrong-level spine surgery (WLS) is a medical error, occurring most frequently in the lumbar spine (71%), followed by the cervical (21%), and the thoracic (8%) spine [4]. WLS has severe consequences, demanding re-surgery, affecting the patient's health and impacting the surgeon's and the team's confidence. In addition, it has significant legal implications; an American study reported that 99% of the WLS cases were subjected to lawsuits, and 54% were settled out of court with indemnity varying between $62.000 and $1.5 million [5].

The conventional approach to performing level localisation during lumbar spinal surgery is palpation, using the intercristal line (Tuffier's line) to identify the L4-L5 intervertebral space. However, multiple studies have identified this landmark as unreliable and variable, reporting accuracies between 29% and 61% [69]–[73]. A survey amongst 105 spine surgeons in the United Kingdom showed that most spinal surgeons (92.4%) use fluoroscopy for level localisation, similar to the reported 86% in a national American survey [74], [75]. Some surgeons (38%) perform a second fluoroscopy image to re-check the level intraoperatively [74]. Although fluoroscopy is a much better technique than palpation, WLS occasionally occurs, reporting incidences of 0.1% to 3.3% [6]–[8]. Moreover, 50-67% of spine surgeons have directly experienced WLS over their careers [4], [75], [76]. Fluoroscopy images are sometimes hard to interpret, especially in obese or older patients with lower bone density. Furthermore, fluoroscopy is associated with disadvantages, using ionising radiation, thereby exposing the patient, surgeon and OR staff to radiation. Moreover, it interrupts the standard surgical workflow as the fluoroscopy system, the C-arm, must be positioned around the sterile field. Furthermore, the surgeon and OR staff must wear lead skirts or stand behind a radiation shielding screen. Ultrasound-based navigation can potentially prevent WLS without using ionising radiation. A mobile ultrasound system can easily be integrated into the standard surgical workflow. Despite these advantages, ultrasound-based spinal navigation is not applied yet in clinical practice, as shown in our literature review (Chapter 2). Baka et al. developed an approach for ultrasound-based level localisation; the Lumbar Localiser [9].

3.1.3. Goals and objectives

This study aims to improve and evaluate the Lumbar Localiser, with the goal of implementing it in clinical practice, replacing the C-arm eventually. It is essential to improve the accuracy and user-friendliness of the approach so it will be adopted in clinical practice. The current approach only allows X-ray as preoperative images. We included MRI since this is the modality of choice to evaluate LSS and disc pathology. Second, we developed a workflow for intraoperative ultrasound acquisition to provide an extra acquisition to verify the level of surgery. Solely use of preoperative ultrasound might cause wrong-level localisation, depending on the angle of the ultrasound transducer (Figure 3.4). Intraoperative ultrasound is performed after incision, thereby eliminating the subcutaneous fat layer. Furthermore, we conducted a clinical study to evaluate the accuracy of the ultrasound-based level localisation. We gathered the opinion of surgeons and OR staff on the pitfalls, opportunities and potential of the approach.
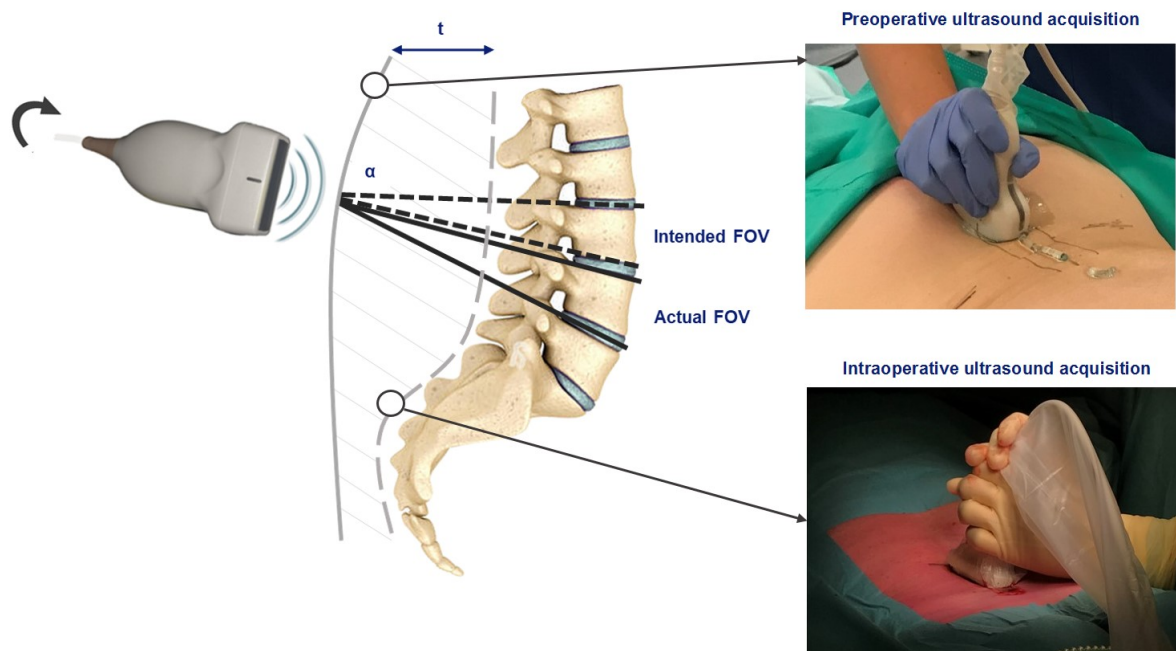
Figure 3.4: Schematic overview of the effect of the thickness *t* of the subcutaneous fat layer on the level localisation during preoperative ultrasound acquisition. A small angle α may result in a changing field of view (FOV), risking wrong-level surgery. Intraoperative ultrasound acquisition eliminates the thickness *t*, as it is performed after incision. Thereby, the effect of the angle α is minimal since the acquisition is on the thoracolumbar fascia, close to the spinous process

3.2. Methods

A clinical study was initiated and performed to evaluate the Lumbar Localiser during surgeries. The Lumbar Localiser was improved and adjusted to fit the clinical workflow of the included institutes. In this section, we describe the study population, image data and Lumbar Localiser. Moreover, we explain the workflow of pre- and intraoperative ultrasound acquisition and our method to evaluate the accuracy of the Lumbar Localiser.

3.2.1. Study population

This multi-centre, prospective study was conducted in the Erasmus MC and the Maasstad Hospital in Rotterdam, the Netherlands. A letter waiving ethical approval was obtained from our institution's Institutional Review Board (IRB). Inclusion criteria were as follows: 1) patients scheduled for open, posterior, lumbar spine surgery; and 2) a minimum of one SP caudal or cranial to the level of surgery. Eligible subjects were identified using the OR planning in the electronic health record (EHR). In the weeks before surgery, patients received the patient information folder and were asked to participate in the study during their visit to the preoperative screening outpatient. We called patients the day before surgery to ask if there were any questions regarding their participation in the study. Written informed consent was obtained on the morning of the surgery. Age and body mass index (BMI) were retrieved from the EHR.

3.2.2. Imaging data

Preoperative imaging (MRI, computed tomography (CT) or X-ray) of the lumbar spine acquired as part of regular clinical workflow was retrieved and pseudonymised. The fluoroscopy images acquired by the C-arm during surgery were retrieved from the EHR. We measured the thickness of the subcutaneous fat layer, including any scar tissue, on MRI. The thickness perpendicular to the skin surface was measured for each SP in MeVisLab.

The imaging modality with the best view of the sagittal SP contours and surgery area was chosen if multiple images were available. We manually drew the contours of the lumbar SP on the chosen sagittal slide in the ultrasound-based navigation software (Figure 3.5). Only the posterior surface of
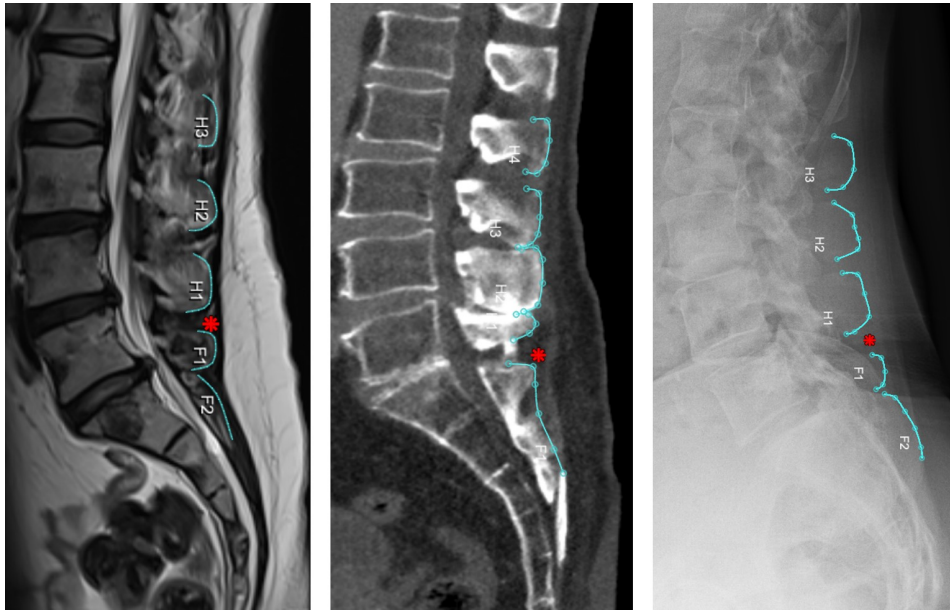
Figure 3.5: Manually drawn contours (blue) on MRI, CT and X-ray; from left to right. The red star sign indicates the intended level of surgery and the tool assigns unique labels (F2, F1, etcetera) to each contour.

the SPs was annotated since that part is visible on ultrasound images. SPs that were removed during previous surgery were not annotated. An experienced neurosurgeon was consulted to confirm ambiguous contours. Subsequently, the desired level of surgery was indicated in the tool. The software then assigned unique labels to each manually drawn contour based on its relative position to the level of surgery (Figure 3.5).

3.2.3. Lumbar Localiser
Software
We used the level localisation approach proposed by Baka et al. as baseline method, as implemented in the Lumbar Localiser MeVisLab tool (Figure 3.6) [9]. We refer to this paper for an in-depth description of the method. In short, this method enables level localisation using preoperative, sagittal ultrasound images. This method is based on the difference in shapes of the SP. A deep learning-based bone segmentation algorithm is embedded in the tool to provide near real-time, automatic segmentation of the SP on the ultrasound images. Subsequently, these segmented images are matched to manually annotated preoperative images using a pair-wise, intensity-based registration. Then, the best match between the consecutive ultrasound and preoperative contours is selected from a similarity matrix. Finally, the labels of the preoperative contours are translated to the corresponding ultrasound images.

We implemented several improvements to the Lumbar Localiser. First, the tool was extended to MRI and CT as preoperative images instead of only X-ray images. This is an improvement as MR images are the preferred diagnostic images for LSS and herniated discs. The approach of Baka et al. had limited use in clinical practice since X-ray images are not standardly acquired for a lumbar surgery indication. It is undesirable to acquire the X-ray images as work-up to the Lumbar Localiser since ionising radiation is used. The second significant improvement was adding the pixel size calculation in the user interface of the Lumbar Localiser. By manual pixel size calculation, a frame grabbing connection between the software and the ultrasound system can be established. Previously, the tool received the ultrasound images via a proprietary protocol over an ethernet connection. This protocol is a DNL connection and provides pixel size information. As this protocol was unavailable on the ultrasound systems at the Maasstad hospital, we used frame grabbing as an alternative connection. Third, we added a manual contour interface to correct ultrasound contours in cases where the segmentation algorithm fails. The last improvement was the option to delete earlier acquired segmentations and their corresponding position during an acquisition. Previously, this was only possible for the most recent ultrasound segmentation, thereby restricting an iterative acquisition process.
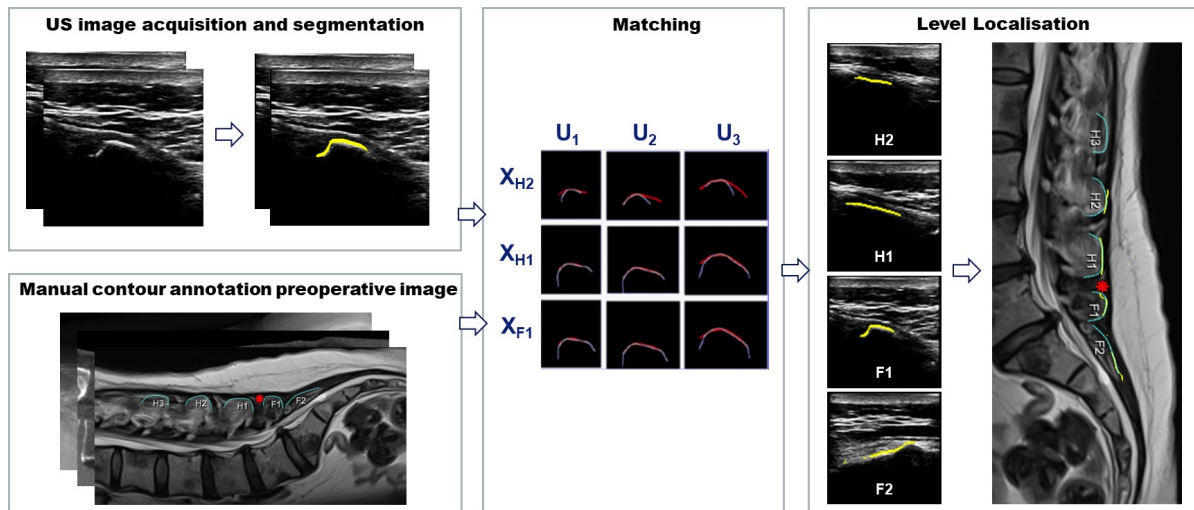
Figure 3.6: The ultrasound-based localisation system. The spinous process shapes from the 2D ultrasound (US) acquisition and the preoperative image are compared and matched. The preoperative image can be an MR, CT or X-ray image. Subsequently, the ultrasound images are labelled by propagating the preoperative image labels to the ultrasound image. The image on the right shows the matched ultrasound contours on the preoperative image, thereby indicating the level of surgery using ultrasound.

Figure 3.7: The used ultrasound transducers. From left to right: Philips L15-7io broadband compact linear array transducer; Philips L12-4 broadband linear array transducer; and Philips C6-2 broadband curved array transducer.

Hardware

The lumbar localisation software runs in MeVisLab 3.0.2. on a research laptop. We connected a foot panel to the laptop to capture snapshots directly without moving the transducer. Different ultrasound systems were available in the two hospitals with corresponding connections. In the Erasmus MC, the Philips iU22 xMATRIX ultrasound system was connected with the DNL connection to the research laptop [77]. The Philips Sparq system was used in the Maasstad hospital with a frame grabbing connection using the Epiphan AV.io HD™ capture card [78], [79]. The frame grabbing connection was used because the DNL connection was unavailable on the Philips Sparq system. Three different 2D transducers were used for ultrasound acquisition: Philips L12-4 broadband linear array transducer; Philips C6-2 broadband curved array transducer; and Philips 'hockey stick' L15-7io broadband compact linear array transducer (Figure 3.7).

3.2.4. Preoperative ultrasound acquisition

The preoperative ultrasound acquisition aims to determine the incision site. The workflow of the ultrasound-based localisation is described in Figure 3.8. Once we arrived at the OR, we connected the frame grabbing or ethernet cables to the ultrasound system and the research laptop (Figure 3.9). Then, the patient received general anaesthesia and was put in a prone position on the surgery table. We palpated the iliac crest to estimate L4-L5 intervertebral space. Ultrasound gel and a condom were applied to the L12-4 and C6-2 transducers, and the gel was applied to the patient's spine. The desired depth

was set on the ultrasound system using an estimation of the depth of the SP based on preoperative imaging. The Philips iSCAN image optimisation was used to automatically adjust time gain compensation (TGC) and receiver gain to achieve optimal uniformity and brightness of tissues. When a frame grabbing connection was used, a reference arrow was drawn with the same length as the depth ruler of the ultrasound system to calculate the corresponding pixel size.

The ultrasound acquisition started with an overview of the SP positions in the sagittal plane, either with the L12-4 or C6-2 transducer. The C6-2 transducer was only used in complex cases (BMI >30 kg/m^2 or re-surgery) to provide an extra overview of the lumbar spine. We first started with acquiring the most caudal SP, the sacrum. We used the L12-4 transducer because the segmentation algorithm only segments SP acquired with linear transducers since it was not trained for convex C6-2 images. Once a SP was located in the centre of the sagittal ultrasound image, a snapshot was taken by pressing the foot panel connected to the laptop. We visually examined the ultrasound segmentation in the tool without moving the transducer on the patient's body. When considered sufficient, the position was marked on the body by indicating a small stripe and number at the centre of the ultrasound transducer (Figure 3.10). If considered insufficient, the transducer was slightly angled to acquire a better image of the SP, and the segmentation was reviewed again. In cases where the segmentation of a SP was still insufficient after adjustment, the segmentation was manually drawn in the tool. After a SP was sufficiently acquired and marked, we slowly moved the ultrasound transducer cranial to acquire the next SP. This process of finding the SP, taking the snapshot, evaluating the segmentation and marking the position on the patient's body was repeated for several levels cranial to the sacrum. The number of levels depended on the desired level of surgery.

Subsequently, we evaluated the matching of the ultrasound contours to the preoperative contours in the tool and manually adjusted the matching if we disagreed with the algorithm proposal. We performed prospective matching on the OR when the matching was considered correct. We used the correspondence between the marks on the patient's body and the preoperative labels to locate the potential incision site. We confirmed the position by repeating the ultrasound acquisition and qualitatively compared these newly acquired SP contours to the previously acquired contours matched to the level of surgery. After this confirmation, we indicated the level of surgery with a cross on the patient's body (Figure 3.10). Retrospective matching was performed after the surgery when prospective matching could not be performed because of a learning curve or time pressure.

Depending on the neurosurgeon's workflow, a preoperative fluoroscopy image was acquired using the C-arm. For those cases, it was directly evaluated whether the proposed level of surgery using the localisation software was correct. A surgical knife or needle was used to verify the exact position of the intended level with the C-arm. Some neurosurgeons only acquired intraoperative fluoroscopy images, basing their incisions on palpation of the patient's anatomy.

3.2.5. Intraoperative ultrasound acquisition

The intraoperative ultrasound acquisition aims to confirm the level of surgery. This acquisition was performed right after the incision and hemostasis before opening the thoracolumbar fascia. The incision area was filled with sodium chloride to enable ultrasound wave transmission. The intraoperative acquisition was performed with the L12-4 and the L15-7io transducer. In cases where the incision was too small for the L12-4 transducer, only the L15-7io transducer was used. The ultrasound images were acquired in the sagittal plane, using a fixed depth of 3 cm and iSCAN image optimisation. The gel and condom were removed from the transducers, and sterile gel and ultrasound covers were applied instead. Similar to the preoperative acquisition, the acquisition started on the caudal site. After a SP was identified, captured with a snapshot and segmented, the acquisition continued on the cranial side. All SPs in the incision area were imaged. The matching of the intraoperative ultrasound contours with the manually drawn contours on the preoperative images was evaluated.

Prospective matching was performed by indicating the proposed surgery level with a small mark made with a monopolar electrosurgical pencil. The proposed level of surgery was then compared with the indicated level based on intraoperative fluoroscopy. All involved neurosurgeons performed intraoperative fluoroscopy to ensure they were at the correct level before starting irreversible bone removal.
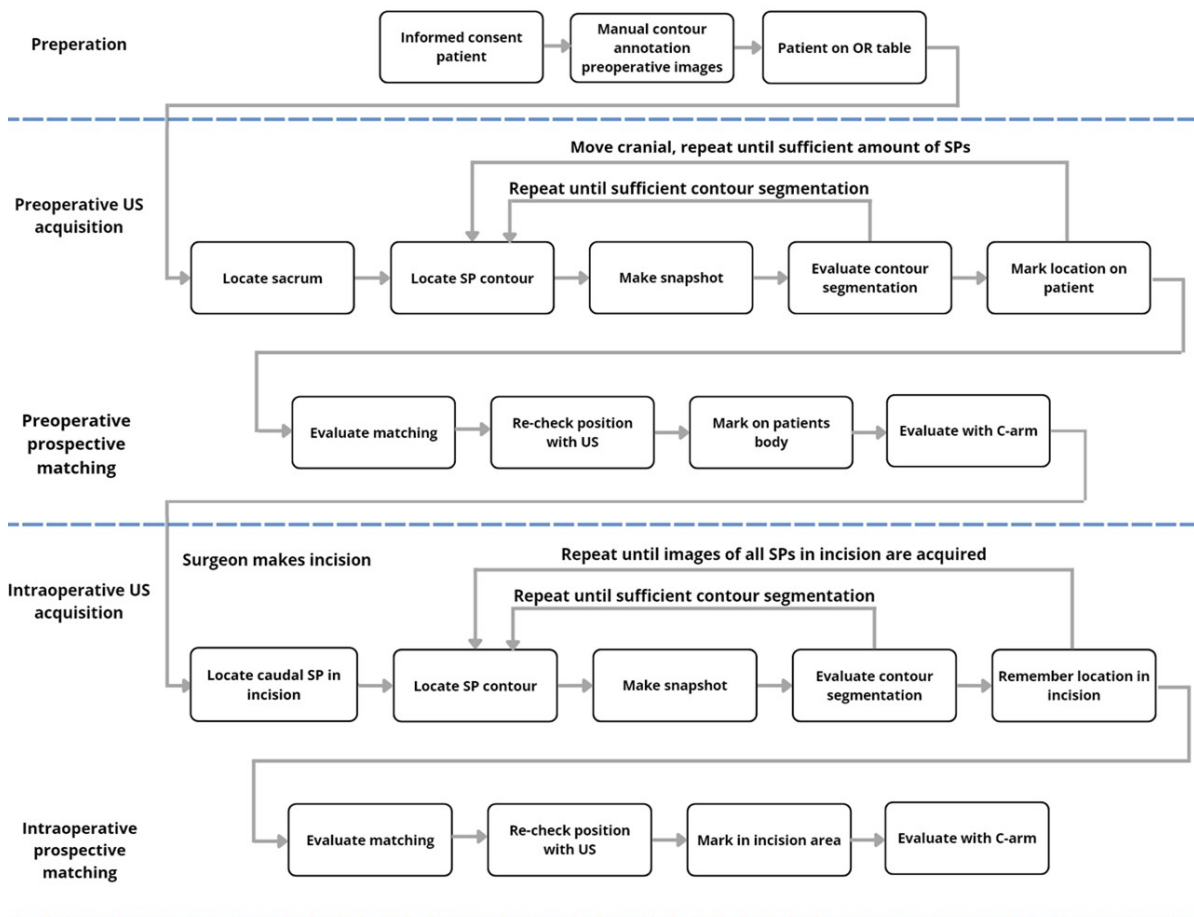
Figure 3.8: Schematic workflow of the clinical study. First, the preparation phase, then the preoperative and intraoperative ultrasound acquisition. SP, spinous process. US, ultrasound.

Figure 3.9: Set-up in the operation room for the ultrasound-based level localisation approach, performing preoperative ultrasound acquisition.
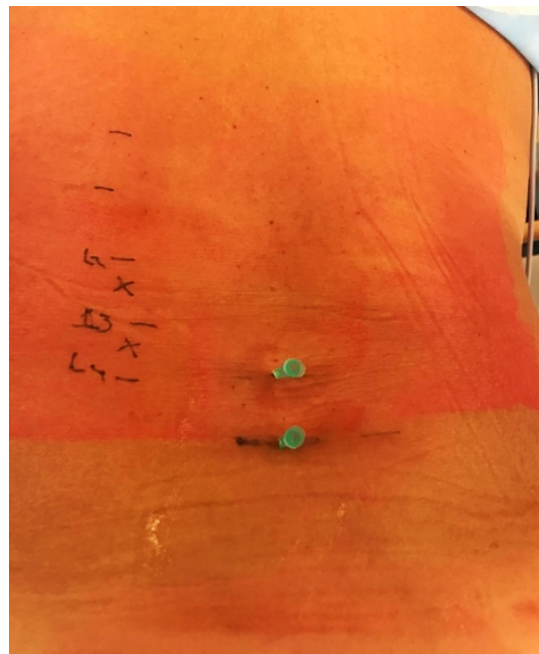
Figure 3.10: Translation of the levels as indicated in the Lumbar Localiser to the patient using marks on the patient's body. Needles are used to verifying the C-arm position.

3.2.6. Evaluation

We recorded the acquisition time of all ultrasound and fluoroscopy acquisitions. We interviewed neurosurgeons, anesthesiologists and OR staff about the potential of ultrasound-based localisation and the advantages and disadvantages of the C-arm. The ultrasound-based level localisation was evaluated using six categories described in Table 3.1. In case a learning curve was observed for ultrasound acquisition and level localisation, a separate analysis was performed to evaluate the performance before and after the learning curve phase. Statistical analysis using the paired T-test was performed in SPSS to calculate differences between the duration of the ultrasound and fluoroscopy acquisition. A p-value <0.05 was considered statistically significant.

Table 3.1: Evaluation categories of ultrasound-based level localisation.

| Category	Acquisition	Segmentation	Matching
A	Incorrect	Incorrect	Incorrect
B	Poor	Incorrect	Incorrect
C	Correct	Incorrect	Incorrect
D	Correct	Correct	Incorrect
E	Correct	Correct	Correct
X	Acquisition not performed		

3.3. Results

3.3.1. Study population

Ultrasound acquisitions were performed in 34 patients (median age 63.5 years old, 61.8% male, median BMI 29.4 kg/m^2) scheduled for lumbar spine surgery. Most surgeries were performed for stenosis (64.7%), and the most common level of surgery was L4-L5 (38.2%). Patient characteristics are presented in Table 3.2.

Ultrasound acquisitions were performed in the Erasmus MC with the Philips iU22 xMATRIX ultrasound system (n=2) and in the Maasstad hospital with the Philips Sparq ultrasound system (n=32). The frame grabbing connection was used in 33 patients and the DNL connection in one patient since the DNL connection could not be established for one patient in the Erasmus MC. Preoperative images were MRI (n=32), CT (n=1), or X-ray images (n=1). Four neurosurgeons were involved in this study: EvP (n=13, 38.2%), JS (n=11, 32.4%), SL (n=9, 26.5%), and RB (n=1, 2.9%). The preoperative ultrasound acquisitions were all performed by the involved researcher, JHS. The intraoperative ultrasound acquisitions with the L12-4 transducer were either performed by EvP (n=1, 6.3%), JS (n=7, 43.8%), JHS (n=7, 43.8%), or HW, an orthopaedic surgeon (n=1, 6.3%). Intraoperative acquisition with the L15-7io transducer was performed by EvP (n=9, 45%), JS (n=4, 20%), or JHS (n=7, 35%). All acquisitions were processed and interpreted by JHS.

Table 3.2: Patient characteristics (n=34).

Characteristic	Value
Age, years, median (Q_1 - Q_3)	63.5 (58 - 73.5)
Gender, female/male, n (%)	13/21 (38.2/61.8)
BMI, kg/m^2, median (Q_1 - Q_3)	29.4 (27 - 31.6)
Depth subcutaneous tissue, cm, median (Q_1 - Q_3)	23.1 (15.2 - 30.8)
Surgery indication - n (%)	
Spinal stenosis	22 (64.7)
Herniated disc	8 (23.5)
Spinal stenosis and herniated disc	4 (11.8)
Type of lumbar surgery - n (%)	
Laminectomy	15 (44.1)
Interlaminair decompression	6 (17.6)
Discectomy	8 (23.5)
Laminectomy and discectomy	3 (8.8)
Interlaminair decompression and discectomy	1 (2.9)
Posterior lumbar interbody fusion	1 (2.9)
Level of surgery - n (%)	
L1-L2	0 (0)
L2-L3	2 (5.9)
L3-L4	5 (14.7)
L4-L5	13 (38.2)
L5-S1	4 (11.8)
Two or more levels of surgery - n (%)	10 (29.4)
Previous lumbar surgery - n (%)	8 (23.5)
Preoperative images of lumbar spine - n (%)	
MRI	33 (97.1)
CT	8 (23.5)
X-ray	10 (29.4)

Q_1, first quartile. Q_3, third quartile. BMI, body mass index. MRI, magnetic resonance imaging. CT, computed tomography.

3.3.2. Preoperative ultrasound acquisition

We performed preoperative ultrasound acquisition with the L12-4 transducer in all 34 patients. Additional acquisition with the C6-2 transducer was performed in 7 patients (20.6%) to acquire an extra overview in complex cases. Localisation results for the preoperative ultrasound acquisition are provided in Table 3.3. Considering the results of retro- and prospective matching, the matching in the localisation software was correct in 35.3% of the cases (n=12) (Figure 3.11). Reasons for incorrect matching were inconclusive matching (14.7%), incorrect segmentation (8.8%), poor acquisition (29.4%) or wrong acquisition (11.8%). We experienced and observed a learning curve for preoperative ultrasound acquisition in patients 1-17. When we consider the results of the patients after the learning curve, patients 18-34, we observe a correct matching in 52.9% of the cases (n=9). The main reason for incorrect level localisation in these cases is poor acquisition (n=5, 29.4%).

Prospective matching based on preoperative ultrasound was performed from patient 22 onward and was correct in 4 out of 13 cases (30.8%). The mismatch between the indicated level by ultrasound and fluoroscopy was one level caudal (n=6) or one level cranial (n=3). In 3 out of 13 cases (23%), the matching proposed by the algorithm was correct; however, the translation to the patient was incorrect. In another three cases, it was evident that the Lumbar Localiser was incorrect. Finally, three cases were risky, as everything seemed correct, but the matching was incorrect since a SP was missed, and the algorithm or observer did not detect this.

3.3.3. Intraoperative ultrasound acquisition

L12-4 transducer

We performed intraoperative acquisition with the L12-4 transducer in 47.1% of the cases (n=16). This ultrasound acquisition could not be performed in the other cases because the incision was too small for

Table 3.3: Localisation results of preoperative ultrasound acquisition with the L12-4 transducer. Values are displayed in n (%) of the number of acquisitions performed.

Category	All patients, n=34	Learning curve, n=17	After learning curve, n=17
A	4 (11.8)	4 (23.5)	0 (0)
B	10 (29.4)	5 (29.4)	5 (29.4)
C	3 (8.8)	2 (11.8)	1 (5.9)
D	5 (14.7)	3 (17.6)	2 (11.8)
E	12 (35.3)	3 (17.6)	9 (52.9)

Category A: incorrect acquisition, segmentation and matching. B: poor acquisition, incorrect segmentation and matching. C: correct acquisition, incorrect segmentation and matching. D: correct acquisition, correct segmentation, incorrect matching. E: correct acquisition, segmentation and matching.

Table 3.4: Localisation results of intraoperative ultrasound acquisition with the L12-4 transducer. Values are displayed in n (%) of the number of acquisitions performed.

Category	All patients, n=16	Learning curve, n=6	After learning curve, n=10
A	1 (6.3)	1 (16.7)	0 (0)
B	3 (18.8)	2 (33.3)	1 (10)
C	4 (25)	1 (16.7)	3 (30)
D	2 (12.5)	2 (33.3)	0 (0)
E	6 (37.5)	0 (0)	6 (60)

Category A: incorrect acquisition, segmentation and matching. B: poor acquisition, incorrect segmentation and matching. C: correct acquisition, incorrect segmentation and matching. D: correct acquisition, correct segmentation, incorrect matching. E: correct acquisition, segmentation and matching.

the transducer (n=17, 50%), or the tight OR schedule did not allow for a second intraoperative acquisition (n=1, 3%). Intraoperative acquisition with the L12-4 transducer showed a correct matching in 37.5% (n=6), considering the retro- and prospective matching (Table 3.4) (Figure 3.12). The other matchings were incorrect because of the following reasons: inconclusive matching (12.5%), incorrect segmentation (25%), poor acquisition (18.8%) or wrong acquisition (6.3%). A learning curve was observed until patient 14. When we only consider the patients after the learning curve (patients 15-34), 60% of the cases resulted in correct matching (n=6). The remaining cases had an incorrect segmentation despite a proper acquisition (n=3) or had poor acquisition of the SP (n=1).

Intraoperative prospective matching with the L12-4 transducer was performed from patient 23 onward, with correct prospective matching in 5 out of 6 patients (83.3%). In the remaining case, it was evident that the Lumbar Localiser proposed an incorrect matching, as the ultrasound segmentation was incorrect.

L15-7io transducer
The L15-7io transducer was unavailable during the first 14 patients (41.2%). Acquisitions were performed in the remaining 20 patients, with a correct matching in 10 patients (50%) (Figure 3.12). A poor acquisition was the main reason for incorrect matching (n=4, 20%) (Table 3.5). Only one patient was required for the learning phase of this transducer since we already gained experience with intraoperative acquisition using the L12-4 transducer. When we disregard this patient from the results, the matching was correct in 52.6% of the cases.

The prospective matching, live on the OR, was correct in 9 out of 12 cases (75%) using the L15-7io transducer. In the remaining three cases, the ultrasound acquisition and segmentation were poor. This indicated to the user that the Lumbar Localiser would not propose a correct matching.

Table 3.5: Localisation results of intraoperative ultrasound acquisition with the L15-7io transducer. Values are displayed in n (%) of the number of acquisitions performed.

Category	All patients, n=20	Learning curve, n=1	After learning curve, n=19
A	1 (5)	1 (100)	0 (0)
B	4 (20)	0 (0)	4 (21.1)
C	2 (10)	0 (0)	2 (10.5)
D	3 (15)	0 (0)	3 (15.8)
E	10 (50)	0 (0)	10 (52.6)

Category A: incorrect acquisition, segmentation and matching. B: poor acquisition, incorrect segmentation and matching. C: correct acquisition, incorrect segmentation and matching. D: correct acquisition, correct segmentation, incorrect matching. E: correct acquisition, segmentation and matching.

Table 3.6: Acquisition times. Values are displayed in minutes:seconds in mean ± standard deviation values.

Acquisition	Acquisition + prospective matching (min:sec)
Fluoroscopy	3:38 ± 2:18
Preoperative ultrasound L12-4	4:59 ± 1:59
Intraoperative ultrasound L12-4	2:10 ± 0:55
Intraoperative ultrasound L15-7io	1:43 ± 0:60

3.3.4. Acquisition time

The time required for the ultrasound and fluoroscopy acquisition including prospective level localisation is provided in Table 3.6. Preoperative ultrasound acquisitions took significantly longer than fluoroscopy acquisitions (mean 4:59±1:59 vs 3:38±2:18 [min:sec], p=0.003). On the other hand, intraoperative acquisitions with both transducers required significantly less time than fluoroscopy acquisitions (p=0.049 and p=0.020, respectively). The opinion of the involved neurosurgeons and anaesthesiologists was that this time difference in the order of minutes was negligible in the clinical practice.

3.4. Discussion

This study showed that the accuracy of the improved level localisation approach was currently insufficient for implementation in clinical practice. The ultrasound-based approach was successfully integrated into the workflow in the OR. It can potentially be an alternative for fluoroscopy level localisation with the C-arm, but further improvements are required to obtain higher accuracy. Intraoperative ultrasound acquisition was easy to integrate into the surgical workflow and added valuable information on the level localisation. It enabled the surgeon to re-check the intended level of surgery without the attenuating effect of the subcutaneous fat layer between the SP and ultrasound transducer. Therefore, we recommend using pre- ánd intraoperative ultrasound acquisition in ultrasound-based level localisation. Several neurosurgeons and anaesthesiologists commented on this ultrasound-based navigation method's great potential to perform level localisation in spinal surgery.

3.4.1. Preoperative ultrasound acquisition

Preoperative level localisation was correct in 35.4% of the cases before the learning curve and in 52.9% after the learning curve. A high rate of incorrect acquisitions existed during the learning curve phase (23.5%) due to problems with the software interface, as images were not saved (n=2), and issues with the ultrasound system settings, as the gain was incorrectly set (n=2). Moreover, poor acquisitions have a rate of 29.4% in the learning curve phase, as the transverse process was imaged instead of the SP. Considering the phase after the learning curve, we also observe a high rate of poor acquisitions (29.4%) due to several reasons: difficulty in finding SP due to a high BMI (>30 kg/m^2) (n=2), abnormal anatomy and scar tissue due to earlier surgery (n=1), and missed SP during acquisition (n=2). The rate of these poor acquisitions might be reduced by further training the sonographer in ultrasound acquisition. Although it is harder to perform SP acquisition adequately in patients with a high BMI, a radiologist demonstrated that an experienced sonographer could identify them in two cases.
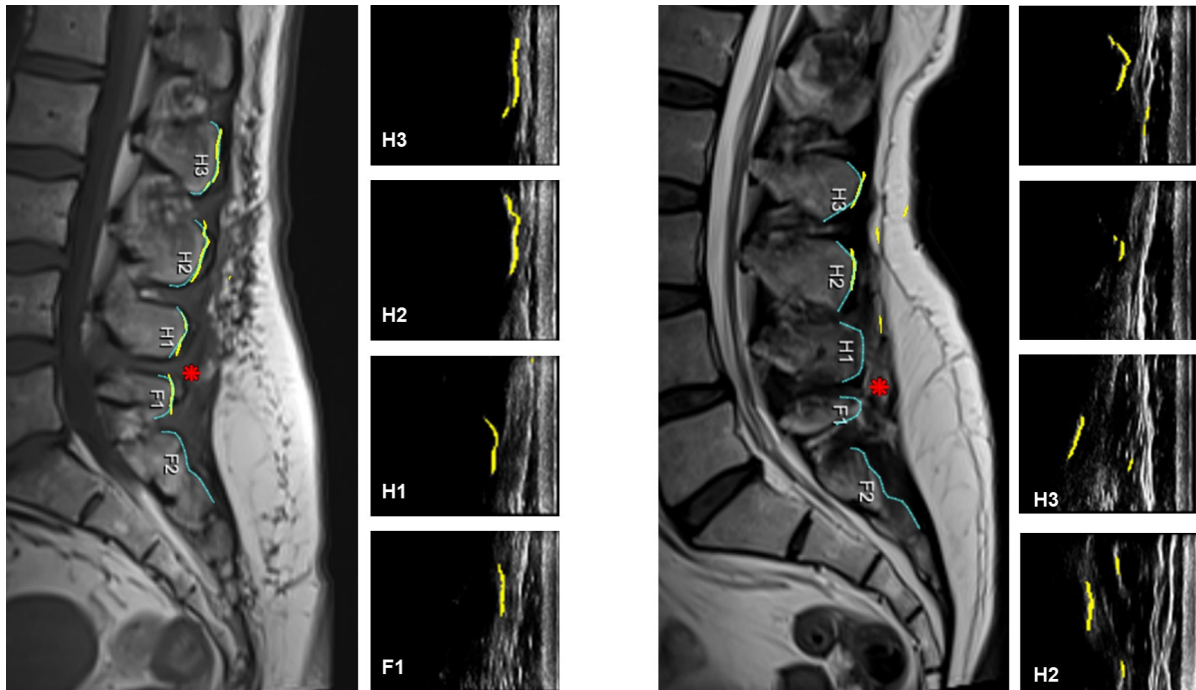
Figure 3.11: Example of two matching cases based on preoperative ultrasound acquisition. Manually drawn contours (blue) of the spinous process (SP) on preoperative MRI and automated segmented SP contours (yellow) on preoperative ultrasound acquisition. Left: correct matching (category E). Right: incorrect matching because of poor ultrasound acquisition (category B).

Figure 3.12: Example of two matching cases based on intraoperative ultrasound acquisition. Manually drawn contours (blue) of the spinous process (SP) on preoperative MRI and automated segmented SP contours (yellow) on intraoperative ultrasound acquisition. Left: correct matching (category E). Right: incorrect matching because of poor ultrasound acquisition (category B).
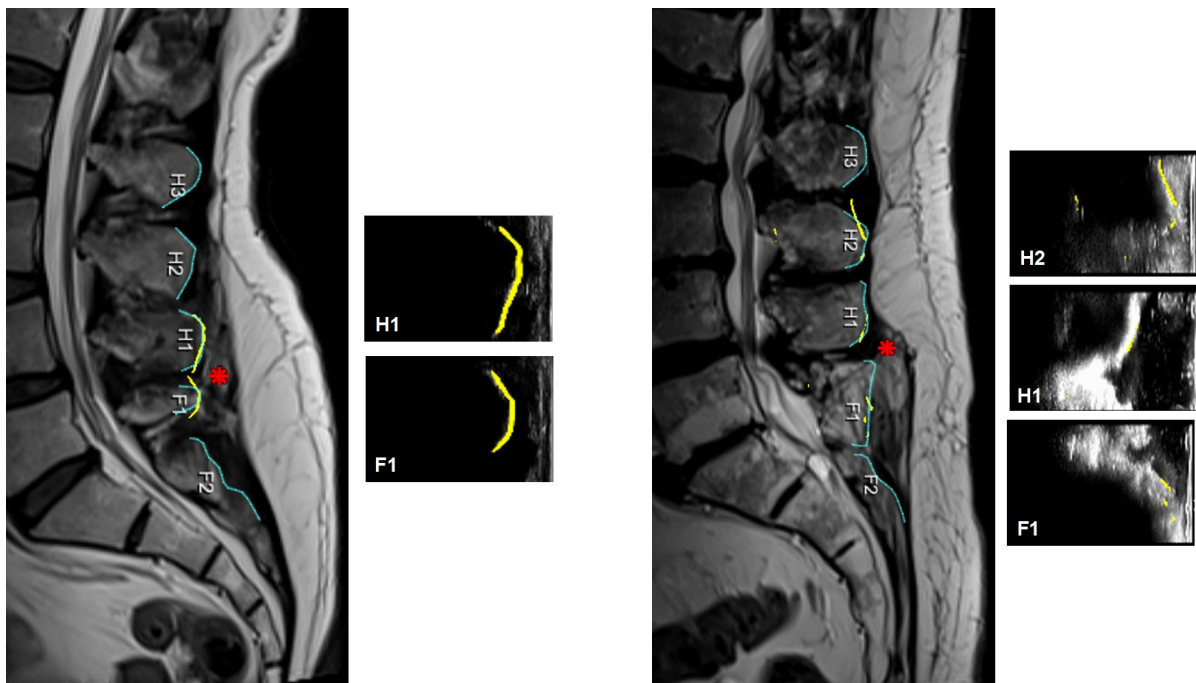
Although ultrasound-based spinal navigation is not applied yet in clinical practice, similar work in a research setting has been published. For example, Baka et al. reported a labelling accuracy of 92% using preoperative ultrasound [9]. Their reported accuracy is higher than our current accuracy, although we used the same software system. Notably, their incorrect and poor acquisition occurs in 8.6% of the cases, while our incidence is 52.9% before the learning curve and 29.4% after. The study setup might explain this difference, as they solely evaluated the matching retrospectively. Moreover, they performed 9 out of 19 included acquisitions (47%) in a more optimal setting; patients in a sitting position in the outpatient clinic. They do not report on the sonographer's experience or an observed learning curve in their study.

The strengths of the preoperative ultrasound acquisition are that it is easy to integrate into the surgical workflow and to acquire an overview of the patient's anatomy. The disadvantage is that it requires training to acquire the images correctly. Also, some cases might be complex, such as obese patients and patients with scar tissue, then SP can easily be missed.

3.4.2. Intraoperative ultrasound acquisition
The intraoperative acquisition was correct in 37.5% of the cases acquired with the L12-4 transducer and in 50% of the cases with the L15-7io transducer, considering all acquisitions. If we only consider the cases after the learning curve, the success rates in level localisation are 60% and 52.6% for the L12-4 and L15-7io transducers, respectively. 3 out of 10 cases (30%) had incorrect segmentation for the L12-4 transducer, which can be explained because the segmentation algorithm was not trained on intraoperative ultrasound acquisitions. However, these cases can be solved by training the segmentation approach on intraoperative ultrasound images. The contours can be manually annotated in the Lumbar Localiser if the segmentation is still insufficient. Another notable result was that 4 out of 19 cases (21.1%) had poor acquisition with the L15-7io transducer. This was due to differed anatomy by earlier surgery (n=1), difficulty in finding the SP (n=2), and time pressure (n=1). The learning curve of intraoperative acquisition required fewer training cases than the preoperative acquisition since we already acquired sonography experience in the other subjects.

Stand-alone intraoperative ultrasound is used in clinical practice to localise and remove the lesion during spinal surgery without disturbing the surgery flow [80]. To the author's knowledge, this is the first study with human subjects which performs intraoperative ultrasound-based spinal navigation. Gueziri et al. evaluated intraoperative ultrasound-based navigation for spine neurosurgery in a porcine cadaver study [81]. They used a tracked transducer to match the ultrasound image positions to preoperative CT images, reporting an overall accuracy between 1.42 and 1.58 mm [81]. However, a disadvantage of their method is that expensive external trackers are required. Therefore, we prefer the currently used image-based ultrasound-based level localisation.

The strength of intraoperative ultrasound-based localisation is that it provides extra information and confirmation. We recommend always using it in combination with preoperative ultrasound localisation. The combination of preoperative and intraoperative acquisition is meaningful, as it provides information about the appearance of the different SP during two ultrasound acquisitions. We advise using the L15-7io transducer in future research, as the results between the two transducers are comparable, and the L15-7io can always be used, while the L12-4 transducer can only be used when larger incisions are made. A disadvantage of intraoperative acquisition is that it can only be done after the incision, meaning that an initial incision side determination must already be performed. Moreover, orthopaedic surgeons might be hesitant to use intraoperative ultrasound in spinal fusion surgery, fearing infection.

3.4.3. Prospective matching
To our knowledge, prospective ultrasound-based spinal navigation in the OR has not been described before in the literature. The main results were that the preoperative prospective matching was correct at 30.8%, and the intraoperative prospective matching at 83.3% and 75% for the L12-4 and L15-7io transducer, respectively. This difference can be explained because the intraoperative ultrasound acquisition is performed as a re-check, meaning more information on the level is already known. Preoperative ultrasound acquisition showed three hazardous cases, as everything seemed correct, but the final level localisation was incorrect. This is dangerous and must be prevented because it gives the physician

confidence that the proposed matching is correct. Moreover, in five cases, the matching proposed by the algorithm was correct; however, the translation to the patient was incorrect. This is because the matching was wrongly interpreted by the user (n=1), or the ultrasound position was improperly translated to the patient (n=4). Also, a learning curve was experienced, as correct translation requires expertise in the relation between the location of the ultrasound image and the transducer.

Correct prospective translation of the matching to the patient is the final step in level localisation. This live matching on the OR was only performed from patient 22 onward because it required extra steps and training in the OR. A disadvantage of the current method of prospective level localisation is that the translation involves a manual step prone to error. Suggestions on improving this translation are described in Subsection 3.4.5.

3.4.4. Acquisition time
The mean time for level localisation using fluoroscopy images was significantly shorter than preoperative ultrasound localisation and significantly longer than intraoperative ultrasound acquisition. The intraoperative ultrasound acquisition takes less time than the preoperative acquisition as the transducer is inserted in the incision area. This minimises the amount of SP to be acquired, restricting the transducer's motion and simplifying ultrasound acquisition as the subcutaneous tissue is no longer between the transducer and the SP. Our proposed approach includes pre- and intraoperative ultrasound acquisition and will take approximately 3 minutes longer than the fluoroscopy acquisition with the C-arm. Although this is a statistically significant difference, it is not considered clinically significant since the involved neurosurgeons and anaesthesiologists considered this time difference negligible.

3.4.5. Further improvements and clinical implementation
Several improvements to the baseline network of Baka et al. and workflow were yet implemented, for example, extension to preoperative MRI, which are described in detail in Subsection 3.2.3 [9]. This section describes further recommendations that may result in better workflow and performance of the Lumbar Localiser for each component of the ultrasound-based navigation: annotation, acquisition, segmentation, matching and translation of the matching to the patient.

Annotation
The annotation step was already significantly improved by extension to MR as preoperative images. However, the tool is not fully automated yet, requiring manual annotation and labelling of the SP contours in the preoperative image. Although less than a minute of work per image, it might introduce performance variability in different users. We developed a deep-learning-based approach to automate the SP contour extraction in Chapter 4.

Acquisition
Several significant improvements were yet accomplished for the ultrasound acquisitions, for example, developing a workflow to perform intraoperative acquisitions. A further suggestion to improve the current ultrasound-based spinal navigation tool is to incorporate axial acquisition. The existing software uses sagittal images, as the different shapes of the SP are visible in the sagittal plane. However, axial acquisition is more straightforward than sagittal ultrasound acquisition since axial acquisition can be performed in one continuous sweep. Sagittal SP shapes should be reconstructed based on the axial images to enable axial acquisition. The preferred tracking method is image-based, therefore not requiring expensive or cumbersome external tracking hardware. Prevost et al. created 3D freehand ultrasound reconstructions based on 2D transducers using deep learning, showing minimal median errors of 3.4% [82]. However, they do not report the computation time in their study. A short computation time of less than a minute is essential to enable near real-time level localisation on the OR. Future research should investigate this application

A second recommendation is directly integrating the Lumbar Localiser into the ultrasound system. This integration replaces the current inconvenient construction, as shown in Figure 3.9. An easier acquisition is facilitated, as the user does not have to switch focus between the research laptop and the ultrasound system. A foot panel would still be connected to the ultrasound system to capture snapshots without

moving away from the transducer. This proposed integration requires collaboration with ultrasound system manufacturers and facilitates the widespread use of ultrasound-based localisation.

Finally, we recommend changing the acquisition workflow by performing additional preoperative ultrasound acquisition on the neurosurgical ward. The ward physician will perform this acquisition, and the surgeon will validate the indicated levels at the OR. An advantage of this workflow is that the ward physician has more time to identify the spinal levels, as there is less time pressure on the ward compared to the OR. Moreover, patients for which the SP are difficult to acquire can be identified early. Then, a more experienced sonographer can be consulted to perform the ultrasound acquisition, or the surgeon can decide to use fluoroscopy-based level localisation. A third advantage is that this workflow allows two physicians to confirm the desired level of surgery, minimising WLS. Disadvantages of this workflow extension are that more physicians must be trained for ultrasound-based navigation and that it involves an extra task for the ward physicians.

Segmentation

We have several recommendations to improve the U-Net bone segmentation algorithm developed by Baka et al. [9]. First, additional training of the segmentation algorithm on intraoperative SP images may improve the segmentation performance. The algorithm showed similar results for pre- and untrained intraoperative correct segmentations (38.2% versus 43.8% and 30.0%).

A second recommendation to improve the Lumbar Localiser using segmentation is to train the algorithm on convex ultrasound images acquired by the C6-2 transducer. The extension to convex images makes the tool more user-friendly, as the user can acquire the SP with the preferred transducer. Moreover, it makes the tool more suitable for complex cases, as the SP are easier to identify with a convex transducer than a linear transducer.

Matching

We propose several adjustments to improve the matching in the current tool. The present method ignores valuable information about the shape of the SP contours on ultrasound images. It only matches the intraoperative contours to the annotated contours of the preoperative X-ray, MRI or CT images. We recommend linking the segmented contours of the intraoperative ultrasound acquisition to the contours of the earlier preoperative ultrasound acquisition. This additional matching option may improve the correct matching in the intraoperative images.

Second, we can improve intraoperative matching by adding context information. As these images are acquired in the incision area, the level of the acquired SPs is constrained to approximately two levels caudal and cranial to the level of surgery. Weighing the position of surgery in the similarity matrix of the matching strategy may reduce the number of incorrect initial matching by the algorithm.

Third, use the sacrum as a reference point for preoperative ultrasound acquisition by weighing the position of the more caudal SP to the sacrum position. The sacrum is larger and has a distinctive shape compared to the lumbar SP; therefore easy to identify using ultrasound. A correct matching between the ultrasound and the preoperative image is more specific for the sacrum.

Fourth, a minimum value for the matching correspondence should be implemented, ensuring more specific matching. The current matching method indicates a matching, even if the segmentations are entirely incorrect. It is crucial to gain the physician's trust in the tool's performance by only suggesting a match when the proposed matching is plausible.

Finally, we propose developing parameters that provide the surgeon with an indication of the correspondence between the ultrasound and preoperative contours. This can be translated into the tool using colour coding. This metric must be clinically evaluated in future research to ensure its predictive value.

Translation to the patient

We experienced that the translation of the matching in the Lumbar Localiser to the correct position on the patient's body is error-prone because of the user's interpretation. We already implemented a workflow with marks on the patient's body to improve this translation (figure 3.10). To eliminate human interference, we propose to include contour-to-contour matching by performing a second ultrasound acquisition. The contour of the second sweep will be matched to the contours of the previous ultrasound acquisition and, therefore, can precisely indicate the surgery position. This step is currently a qualitative comparison by the user, thereby experiencing difficulties in accurately comparing the contours. To mark

the position on the patient's body precisely, we suggest including corresponding measurement axes on the ultrasound images and transducers. Then, the user can translate the position of the SP or the intervertebral disc precisely to the live situation. This proposal requires collaboration with ultrasound system manufacturers, as the measuring axes must be added to their software and transducers.

3.4.6. Limitations and future research

The first limitation of this study was that the sonographer who performed most acquisitions (69%) was entirely inexperienced with ultrasound acquisitions. Therefore, we expect that the described learning curve of 17 patients will be shorter for neurosurgeons as they have more experience with ultrasound acquisitions. Future research should evaluate the learning curve in neurosurgeons. Second, we have fewer study data on intraoperative acquisitions with the L15-7io transducer, as this transducer was unavailable during the first 14 acquisitions. Since we advise using the L15-7io transducer for intraoperative acquisitions because of the smaller dimension, future research should perform more acquisitions with this transducer. Finally, we used the frame grabbing connection in 32 out of 34 acquisitions (94%), thereby missing image metadata since this connection uses screenshots of the actual ultrasound images. Although we manually added the pixel spacing, this approximation might influence the SP segmentation. We recommend using a direct connection to the ultrasound system in future research, for example, a digital link to the ultrasound system.

3.5. Conclusions

In conclusion, we improved and evaluated an ultrasound-based localisation method for lumbar spinal surgery. Our clinical study showed that the accuracy of the improved level localisation approach was currently insufficient for implementation in clinical practice. The final level localisation workflow achieved an accuracy of 52.9% for preoperative level localisation and 60% and 52.6% for intraoperative level localisation with the L12-4 and L15-7io transducer. The low accuracy is mainly caused by poor SP acquisition, indicating that further sonographer training is required. Moreover, we showed that pre- and intraoperative ultrasound acquisitions could be efficiently integrated into the OR workflow, with clinically negligible time differences. A learning phase was observed to perform the ultrasound acquisitions and prospective matching adequately. In the current study, improvements were yet implemented, including extending to intraoperative ultrasound acquisition, adding MRI as preoperative image modality, enabling frame grabbing connection, developing a manual segmentation interface and developing a prospective matching workflow. Intraoperative ultrasound acquisition added value to the approach, allowing the surgeon to re-check the intended level of surgery without the attenuating subcutaneous fat layer between the SP and transducer.

Future research should further develop the proposed method, incorporating contour-to-contour matching for intraoperative acquisition and translation. Moreover, users should be adequately trained to acquire the SP and interpret the matching. Also, a colour coding should be added to the tool to give the surgeon an indication of the matching certainty. We recommend only using the L15-7io transducer for intraoperative acquisition, as the incisions are often (53%) too small for the L12-4 transducer. Neurosurgeons and anaesthesiologists regard this ultrasound-based navigation method as having a considerable potential to perform level localisation in spinal surgery.

<div style="text-align: right; font-size: 4em;">4</div>
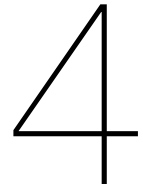
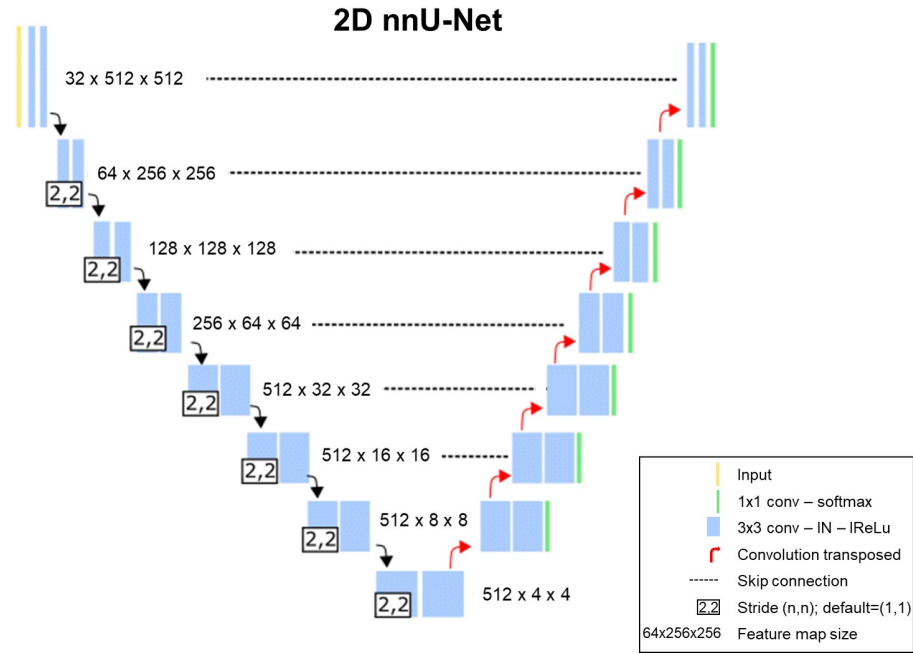# Spinous process contour segmentation in MRI using nnU-Net

4.1. Introduction

Wrong-level spine surgery (WLS) is a medical error with severe consequences for the patient and medical staff [4], [5]. The current golden standard for level localisation is fluoroscopy images acquired by a C-arm. However, this approach uses ionising radiation and interrupts the standard surgical workflow. Ultrasound-based navigation may overcome these disadvantages and may provide an alternative to prevent WLS during spinal surgery. Baka et al. developed the Lumbar Localiser for ultrasound-based level localisation based on the unique shapes of the spinous process (SP) [9]. Detailed information on WLS and the Lumbar Localiser are provided in Section 3.1 and Subsection 3.2.3. In the baseline approach, the contours used for localisation are created by manual annotation on preoperative X-ray images. Although less than a minute of work per image, it might introduce performance variability in different users. An automatic contour segmentation method may reduce the annotation variability and improve performance. In addition, the user-friendliness of the approach may improve as less manual interaction is required. Moreover, the approach may be better applicable in clinical practice when magnetic resonance imaging (MRI) is included as a preoperative imaging modality. MRI is the modality of choice to evaluate spinal stenosis and disc pathology, which are common indications for spinal surgery [83].

This study aimed to develop an approach for automatic contour extraction to be used in the Lumbar Localiser. First, we developed a method for automatic segmentation of the SP based on MRI using deep learning. Second, we created a method to extract the posterior contours based on these segmentations and implemented these in the Lumbar Localiser. We evaluated the performance of our approach by comparing the matching results between automated and manually created contours.

4.2. Methods

The developed approach was based on T2-weighted sagittal MR images since this sequence is the preferred preoperative image for the Lumbar Localiser (Chapter 3). The SPs were segmented using deep learning. A nnU-Net was used as the segmentation approach, as it shows state-of-the-art performance in international biomedical image segmentation competitions [84]–[86]. nnU-Net is based on the U-Net architecture and is a self-configuring approach where preprocessing, network architecture, training, and post-processing pipelines are automatically configured and tuned for any new dataset (Figure 4.1) [84], [87].

First, ground truth annotations were created for each SP on the sagittal slide with the best view of the SP. SPs that could not be annotated because they were removed during previous surgery were excluded. The annotations were preprocessed to convert the 2D data (x,y) to pseudo-3D images (1,x,y) since nnU-Net expects 3D images as input data [88]. Additional preprocessing, such as normalisation and resampling was not required as nnU-Net does this automatically. Data preparation was performed,

2D nnU-Net

$32 \times 512 \times 512$

$64 \times 256 \times 256$

$128 \times 128 \times 128$

$256 \times 64 \times 64$

$512 \times 32 \times 32$

$512 \times 16 \times 16$

$512 \times 8 \times 8$

$512 \times 4 \times 4$

	Input
	1x1 conv − softmax
	3x3 conv − IN − lReLu
	Convolution transposed
------	Skip connection
2,2	Stride (n,n); default=(1,1)
64x256x256	Feature map size

Figure 4.1: nnU-Net architecture.

selecting the slice containing the most annotated SPs. This slice and the corresponding label were used for the segmentation method with entire slices as input (Figure 4.2). For the other method, based on SP regions of interest (ROIs), each ROI was extracted from the entire slice and saved as a separate image. The ROI image of each SP and its corresponding label was used as input for the segmentation network (Figure 4.2).

After segmentation, the posterior SP contours were extracted based on the segmentations resulting from the best-performing nnU-Net approach. These contours were obtained by extracting the first segmented pixel for each row, seen from the dorsal side (Figure 4.3). Subsequently, the contours were refined by a filtering step. This filtering was not applied to the sacrum, as the sacrum has a deviating anatomy compared to the lumbar SP.
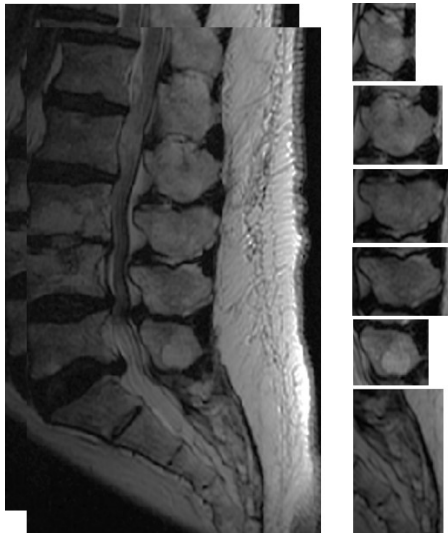

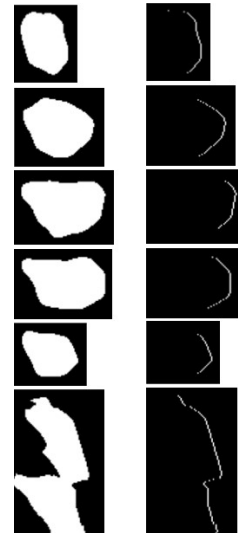**Figure 4.2:** Left: entire sagittal T2-weighted MRI slices. Right: regions of interest of the spinous process.

Figure 4.3: Left: segmented spinous process. Right: the posterior contours are extracted based on the segmentation.
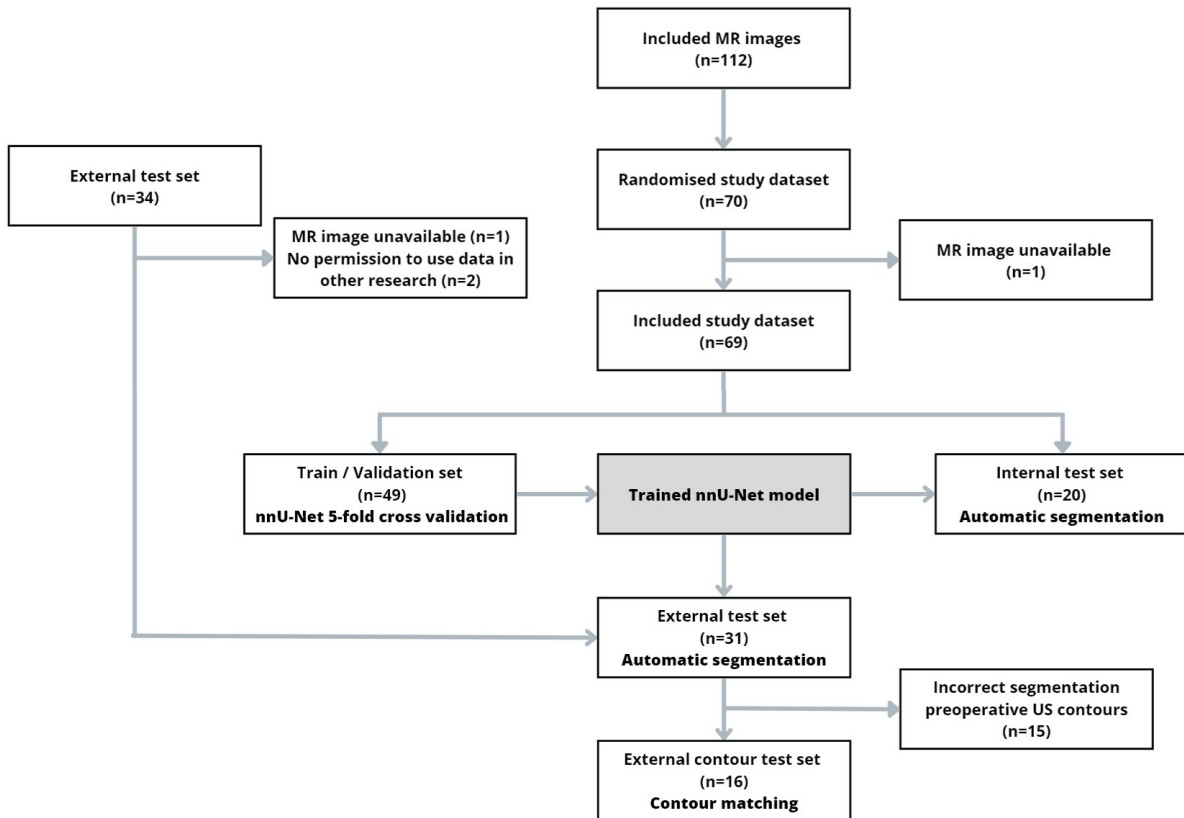
Figure 4.4: Data flow of the patient selection, training and evaluation process. US, ultrasound.

4.3. Experiments

4.3.1. Datasets

Internal dataset

In this retrospective study, we pseudonymised image data acquired during clinical routine from Erasmus MC in Rotterdam, the Netherlands. A letter waiving ethical approval was obtained from our institution's Institutional Review Board (IRB) and written informed consent was waived. We retrieved image data from 112 patients based on the inclusion criteria: 1) MRI of the lumbar spine acquired to examine spinal stenosis or herniated discs; 2) reviewed by one of the involved radiologists (E.O. and H.A.); and 3) acquired between May 2020 and May 2022. Computed tomography (CT) and X-ray images of the lumbar spine were also collected if available for the included patients. 70 patients were randomly selected for the study dataset (Figure 4.4). One patient was additionally excluded, as T2-weighted sagittal MRIs were unavailable. The median age of the participants in the dataset was 63 years, ranging between 22 and 84 years, and 53.6% was female. The median pixel size of the MR images was 0.625 x 0.625 mm^2 and the median slice thickness was 3 mm. Most MR images were obtained using a GE HealthCare (GEHC) Optima MR450W scanner (n=28) and a GEHC SIGNA Artist scanner (n=25). The image data was randomly distributed among a train/validation set (n=49) and a test set (n=20). The train/validation set included 275 SP and the test set 106 SP. MRI and system characteristics are detailed in Table 4.1.

External dataset

We used an external test set with image data from 31 patients with 180 SPs from the clinical study described in Chapter 3. Two patients were excluded because they did not give their permission to use their data in other research, and one patient was excluded as the MRIs were unavailable. The median age of the participants in the external dataset was 63.5 years, ranging between 41 and 85 years, and 38.2% was female. The median pixel size of the images in the external test set was 0.729 x 0.729 mm^2 and the median slice thickness was 4 mm (Table 4.1). Most MR images (n=21) were obtained using

Table 4.1: MRI and system characteristics in the train/validation, internal and external test sets.

	Train/validation set	Internal test set	External test set
Number of MR images	49	20	31
Number of annotated SPs	275	106	180
Median pixel size (mm^2)	0.625 x 0.625	0.625 x 0.625	0.729 x 0.729
Median slice thickness (mm)	3	3	4
Number of hospitals			
Erasmus MC	49	20	2
Maasstad	-	-	16
Other[a]	-	-	13
Number of MRI systems			
GEHC[b]	46	19	1
Philips[c]	3	1	7
Siemens[d]	-	-	23

SP, spinous process. GEHC, GE HealthCare. MRI, magnetic resonance imaging. [a]Ikazia, DC klinieken, Spijkenisse Medisch Centrum, CuraMare. [b]GEHC SIGNA Artist, GEHC DISCOVERY MR750, GEHC SIGNA PET/MR, GEHC SIGNA Premier, GEHC Optima MR450w. [c]Philips Ingenia Ambition S, Philips Achieva dStream. [d]Siemens MAGNETOM Sola fit, Siemens MAGNETOM Essenza, Siemens MAGNETOM Sola, Siemens Symphony.

a Siemens MAGNETOM Sola Fit. Images were acquired at the Maasstad hospital (n=16), Erasmus MC (n=2), or other hospitals (n=13). Ultrasound acquisitions of the SP contours were available for all patients in the external test set. Sixteen patients had correct segmentations of the preoperative ultrasound contours and were included to evaluate the contour matching (Figure 4.4).

4.3.2. Implementation

The nnU-Net models were trained and evaluated on a computer with NVIDIA GeForce GTX 1080 8GB GPU. We applied a 5-fold cross-validation for training and validation to ensure results and training reliability. We did not change the nnU-Net hyperparameters and augmentation strategy. The network was trained with 1000 epochs, the standard number for nnU-Net.

Annotations were performed in MeVisLab 3.0.2 and preprocessing in Python 3.9. JHS manually created ground truth annotations of the sacrum and lumbar SP on the MR images. Data preparation of the method based on ROIs of the SPs started with labelling each SP using the Python package *SciPy* [89]. Subsequently, the ROI of the SP was selected by cropping the image based on the SP dimensions, including a margin of 5 pixels on each side. These same steps were applied to the binary label images with an additional largest component analysis [90]. We evaluated whether the entire sagittal slice or ROIs of the SP resulted in the highest segmentation performance (Figure 4.2).

Postprocessing included filtering the contours by excluding pixels with a y-value larger or smaller than the median y-value of all contour pixels $\pm$ 10 pixels. The created .csv files of the contours were converted to .cso files in MeVisLab and uploaded to the Lumbar Localiser. We only compared the contours of patients with available and correctly segmented ultrasound contours acquired in preoperative ultrasound acquisition.

4.3.3. Evaluation metrics

To quantify the performance of the segmentation models, we used the mean Dice similarity coefficient (Dice Score) as a measure. The Dice score was calculated as follows:

$$\text{Dice score} = \frac{2|A \cap B|}{|A| + |B|} \quad , \tag{4.1}$$

where A is the set of predicted mask pixel locations and B is the set of ground-truth annotated pixel locations. Dice scores range from 0 to 1, where 1 indicates a segmentation that matches the ground truth segmentation for all pixel locations in the segmentation masks. Furthermore, we calculated the 95% confidence interval (CI) on the mean Dice score for each experiment.
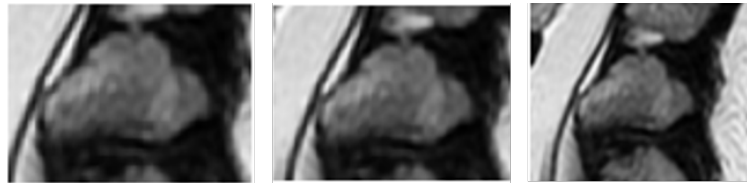
Figure 4.5: Different dimensions of the same region of interest of a spinous process (SP). Left: original cropped SP. Middle: added margin of 10 pixels on each side and an offset of -5 pixels in the y-direction. Right: margin of 20 pixels on each side and an offset of +5 pixels for y.

4.3.4. Experiments

1. Evaluation performance segmentation models
We compared the performance of the segmentation models trained on entire slices with the performance of models trained on SP ROIs.

2. Evaluation training size
We performed a training size evaluation to evaluate whether we used sufficient training data to achieve optimal performance. We created seven additional train/validation sets of different sizes: 1-3) n=10; 4-5) n=20; 6) n=30; and 7) n=40. The number of subjects was randomly selected from the entire train/validation set of 49 patients. Each network was evaluated on the same test set of 20 patients.

3. Evaluation ROI margins
We evaluated the performance of the segmentation model with varying margins of the ROI containing the SP. Twenty variations were created for each SP, with added margins on each side ranging from 5 to 25 pixels (Figure 4.5). Each created SP had an offset of 5 pixels to the centre of gravity in varying directions.

4. Evaluation robustness segmentation model
In our fourth experiment, we validated the robustness of the proposed segmentation model by evaluating the Dice score on an external test set.

5. Evaluation contour matching
We evaluated the quality of the created contours by comparing them with manually created contours. Both were matched to the ultrasound contours in the Lumbar Localiser. The contours were visually inspected for differences between the automatic and manual contours.

4.4. Results

Figure 4.6 shows the pipeline of the proposed contour extraction approach. This section describes the results of each experiment.

1. Evaluation performance segmentation models
The performance of the segmentation model with the entire slices as input achieved a mean Dice score of 0.80 with a 95% CI between 0.78 and 0.83 (Figure 4.7). The other model, trained on SP ROIs, showed a higher performance with a mean Dice score of 0.92 with a 95% CI between 0.91 and 0.93 (Figure 4.8). We used this model with SP ROIs for the rest of the experiments since it achieved a higher segmentation performance.

2. Evaluation training size
Figure 4.9 shows the relation between the training size and model accuracy. The performance of the segmentation model for all levels does not change with a varying training set's size (0.92 n=10 versus 0.93 n=49). Similar constant results are shown when we only consider the lumber and sacral levels (0.94 vs 0.93 and 0.86 vs 0.87, respectively).
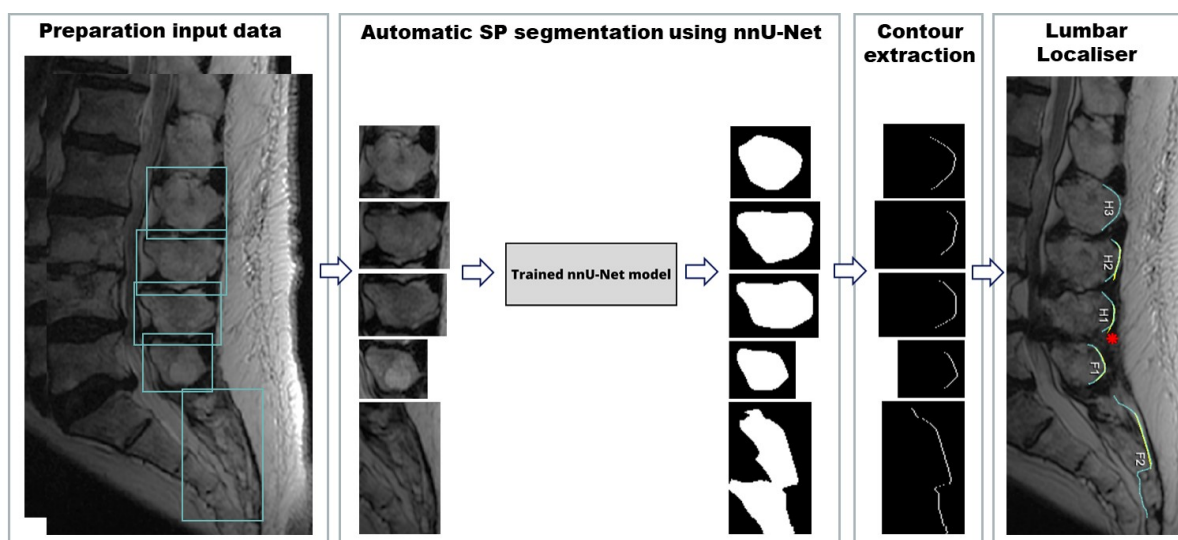
Figure 4.6: Schematic workflow of the proposed contour extraction approach. The first step is to manually prepare the image data, indicating the region of interest of the spinous process (SP). Subsequently, the SP contours are extracted based on nnU-Net segmentations and imported into the Lumbar Localiser. Blue contours: automated created MRI contours; yellow contours: automated segmented contours based on preoperative ultrasound acquisition.
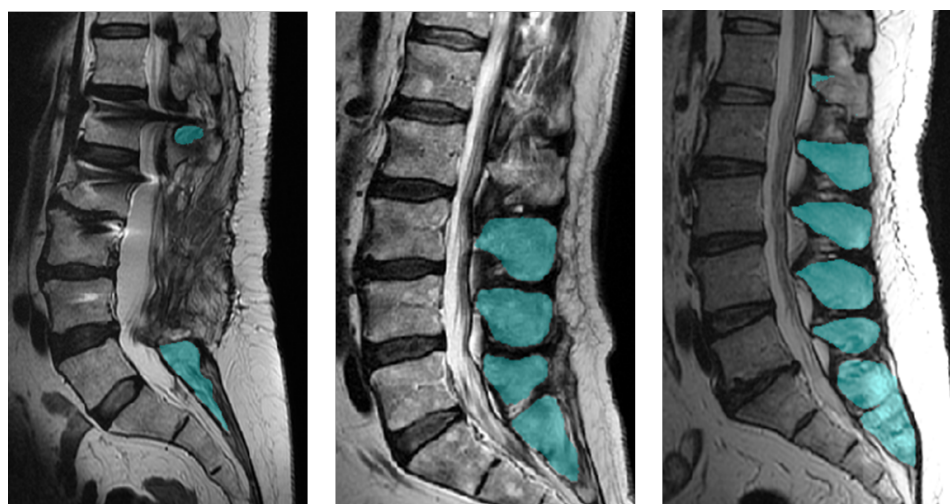

Figure 4.7: Three examples of segmentations (blue) resulting from the nnU-Net trained on the entire T2-weighted MRI slices. Left: correct segmentation, since only the visible spinous process (SPs) are segmented, as L2-L5 are removed during a previous surgery. Middle: correct segmentation since L1 and L2 are not optically visualised in this slice. Right: partly incorrect segmentation, as only a small part of L1 is segmented. This would result in an incorrect posterior contour for L1.
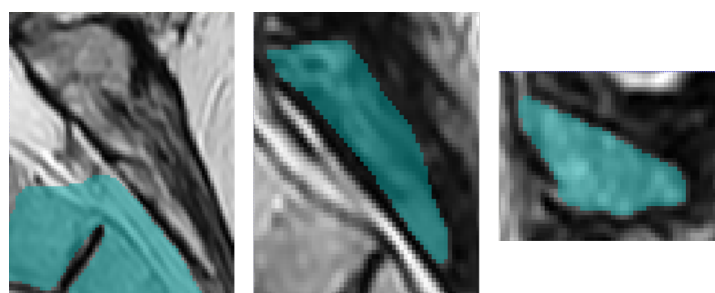

Figure 4.8: Three examples of segmentations resulting from the nnU-Net trained on regions of interest (ROIs) of the spinous process (SP). Left: an incorrect segmentation of the sacrum, as the sacral vertebrae are segmented instead of the SP. Middle: a correct segmentation of the sacrum. Right: a correct segmentation of the lumbar SP, while this segmentation has the lowest Dice score of all lumbar SPs (0.86).
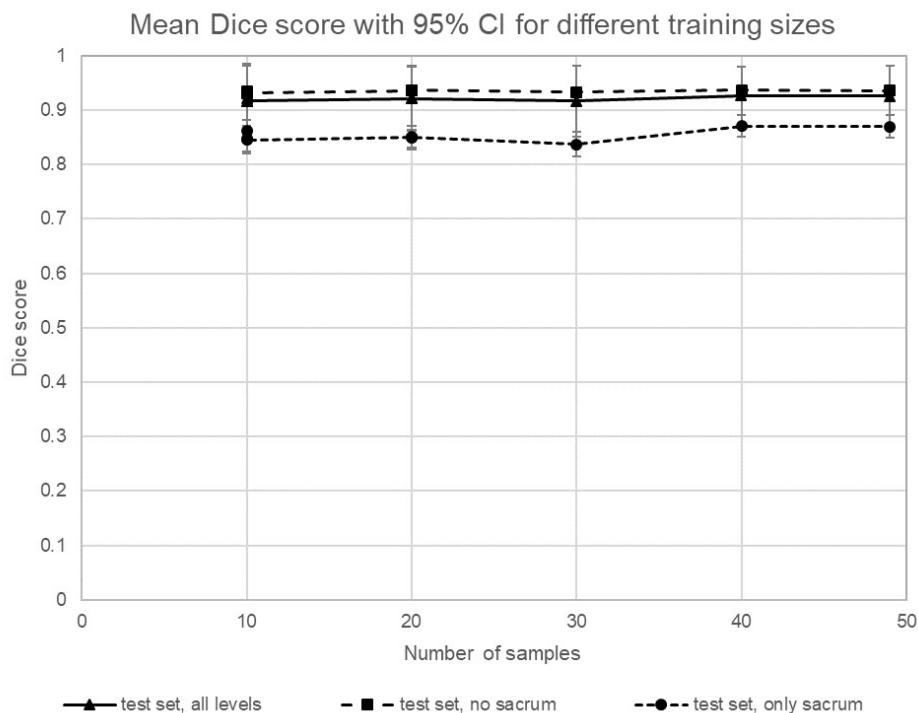
Figure 4.9: Relation between sample size and model accuracy for the trained nnU-Net. Performance is evaluated using the mean Dice similarity coefficients (Dice score) and 95% Confidence Intervals (CI).
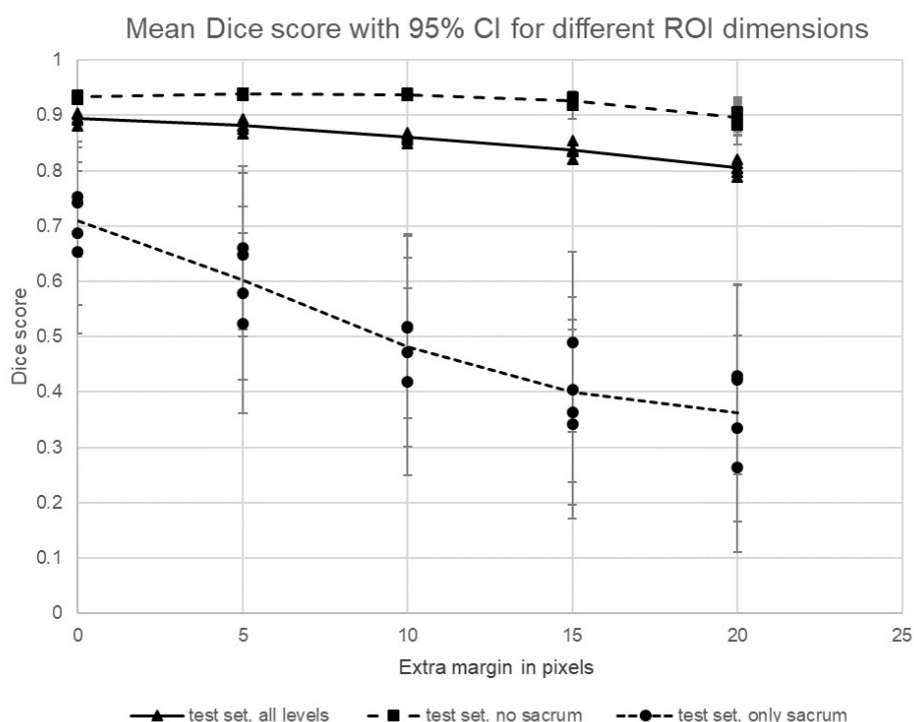

Figure 4.10: Relation between the dimension of the spinous process (SP) regions of interest and model accuracy. Performance is evaluated using the mean Dice similarity coefficients (Dice score) and 95% confidence intervals (CI). Each margin included four data points, as an additional 5-pixel offset from the centre of gravity was applied in +x, -x, +y and -y directions.

Table 4.2: Internal (n=20) and external (n=31) test set results tested on all spinous process (SP), only lumbar and only sacral SP. Performance is evaluated using the mean Dice similarity coefficient (Dice score) and 95% confidence intervals (CI).

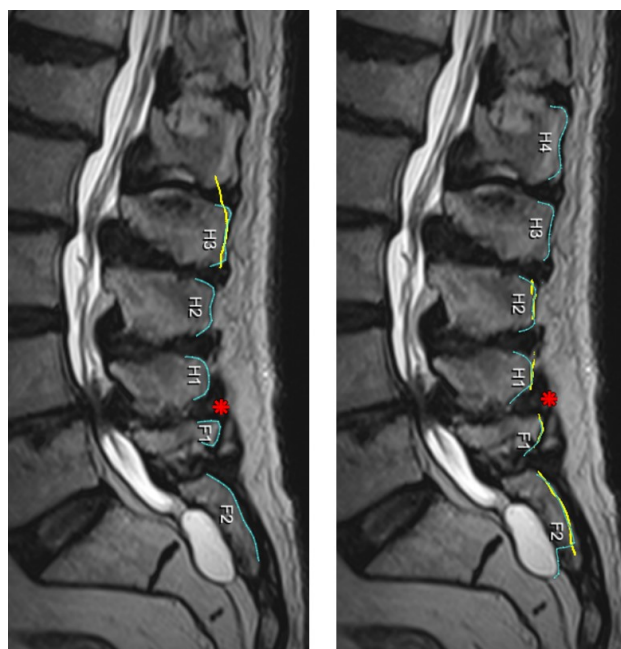|	Internal test set, Dice score [95% CI]	External test set, Dice score [95% CI]
All SPs	0.93 [0.92 - 0.94]	0.86 [0.81 - 0.90]
Lumbar SPs (no sacrum)	0.94 [0.93 - 0.94]	0.93 [0.91 - 0.95]
Sacral SP	0.87 [0.85 - 0.89]	0.50 [0.43 - 0.56]

Figure 4.11: Left: manually annotated contours (blue) and the corresponding matching with the segmented ultrasound contours (yellow). Right: our automated contours (blue) and their matching with the segmented ultrasound contours (yellow) showed an improved initial matching proposal.

3. Evaluation ROI margins

When regarding all levels in the test set, the performance decays from a Dice score of 0.89 to 0.81 when a margin of 20 pixels is added on each side to the 5-pixel offset. (Figure 4.5, Figure 4.10). When we only consider the lumbar SP, excluding the sacrum, the performance does not change when a margin of up to 15 pixels is added (0.93 Dice score). This performance lowers to a 0.89 Dice score when a margin of 20 pixels is added. The performance of the segmentation of the sacrum shows a steep decay with larger margins, with a mean Dice score of 0.71 with a 5-pixel offset, to 0.36 with a 20-pixel additional margin.

4. Evaluation robustness segmentation model

Table 4.2 displays the results of the quantitative evaluation of the model's performance on the internal and external test set. The network achieved 0.93 and 0.86 Dice scores for all SPs of the internal and external test set, respectively. When excluding the sacrum from the analysis, Dice scores of 0.94 and 0.93 were achieved for the internal and external test set. The performance of the model showed a considerably larger difference between the internal and external test set (0.87 versus 0.50 Dice score).

5. Evaluation contour matching

The lumbar SP did not show evident visual differences in all patients, whether the sacrum had a different shape in 6 out of 16 cases. However, this shape difference of the sacrum did not result in an altered proposed matching by the Lumbar Localiser, as the created contours from our automatic approach did not result in any matching differences compared to the manually segmented contours (n=14). The automatic contours improved matching in the remaining two cases (Figure 4.11).

4.5. Discussion

Manual annotation of SP contours requires an extra workload for the user and might introduce user-dependent performance variability. Therefore, we proposed an automatic approach to extract SP contours using segmentations created with a deep learning approach. We compared the matching of the automatically and manually created contours with the ultrasound contours in the Lumbar Localiser. Our approach showed excellent results, as the matching proposed by the Lumbar Localiser did not change in 14 out of 16 cases and even improved the remaining 2 cases. This improvement can be explained as the segmentation model is more consistent in annotation than human users. We did not achieve an optimal performance of the model for the sacrum segmentation in the external test set (0.50 Dice score), which resulted in visually incorrect contours in 6 out of 16 cases. Nevertheless, these inaccurate contours did not result in incorrect matching in the Lumbar Localiser. For example, Figure 4.11 shows an incorrect sacrum segmentation but a correct matching in the tool. The proper matching, despite a low Dice score, can be explained by looking at the sacrum segmentations. The vertebra anterior to the sacrum is frequently segmented by nnU-Net as part of the sacrum (Figure 4.8). This results in a low Dice score, but the posterior contour is minimally affected. The purpose of this study was not to achieve the highest possible performance for SP segmentation but to achieve the highest contour matching in the Lumbar Localiser. Therefore, our approach is applicable for lumbar and sacral SP contour extraction.

We used the segmentation model trained on the SP ROI since this model showed superior results compared to the model trained on entire SP slices (experiment 1). This method requires manual interaction to prepare the data for the segmentation network as the dimensions of the SPs should be indicated (Figure 4.6). Future research should incorporate an object-based segmentation method to eliminate this manual step. Moreover, we recommend evaluating the method based on entire slices more elaborately in future research. Although the Dice score was lower for this method, visual examination shows proper segmentations of the SP on the entire slices. In particular, the sacrum is better segmented in the entire slices than the SP ROIs. The context information of the entire spine prevents additional vertebrae segmentation, as occurred frequently for the SP ROI segmentations. An additional advantage is that manual ROI selection is not required with entire slices as input. Further reduction of user interaction will improve the user-friendliness of the Lumbar Localiser even more. A small manual interaction will always be acquired, as the user has to indicate which lumbar SPs will be included in the ultrasound-based localisation method since not all SPs are required in the Lumbar Localiser.

Experiment 2 showed that the subset of 69 patients was sufficient since the performance did not increase with the addition of more training data. The proposed segmentation model is sensitive to the image data input, especially for the sacrum ROI dimensions, as shown in experiment 3. The sensitivity of the sacrum for enlarging margins can be explained as a larger area of the anterior vertebrae is included in the ROI. As highlighted before, nnU-Net frequently includes this part in the segmentation instead of only the SP, thereby lowering the Dice score. We advise minimising the margin for the sacrum SP ROIs, as the performance shows a steep decay with increasing sacral margins (Figure 4.10). For the lumbar SPs, we advise maximising the margin of the ROIs to 15 pixels. The entire posterior surface of the SPs should always be included in the ROI to extract the correct contours.

To our knowledge, this is the first study which developed a deep learning-based approach for SP segmentation using MRI. We compared our results to other machine and deep learning-based segmentation methods, as shown in Table 4.3. We identified one study which developed a SP segmentation method based on cervical X-ray images using machine learning. They reported a Dice score of 0.88 [91]. Other studies applied a similar method to segment the lumbar spine vertebral bodies, reporting Dice scores close to our results (0.93 and 0.95) [92], [93]. Interestingly, Lu et al. achieved a similar performance for sacral segmentation compared to lumbar segmentation, while our Dice score is lower for sacral segmentation. This difference can be explained by looking at their sacral segmentations. They only segmented the first sacral vertebrae, while we segmented the entire sacral SP, resulting in a different shape than the lumbar region. Moreover, we were the only study that evaluated the results on an external test set to validate the robustness of our proposed segmentation method.

Further research should incorporate a metric that better reflects the posterior contour accuracy. The Dice score evaluates the entire segmentation, resulting in a low score, also when the posterior surface

is not affected as only anterior parts are wrongly segmented. Moreover, future research should focus on the optimal method to incorporate the proposed method in the Lumbar Localiser. The time required to segment 1, 6 and 105 SP ROIs was 5.5, 6.9 and 32.5 seconds. This short time, especially with increasing SPs, enables near real-time segmentation in the Lumbar Localiser.

A limitation of our study is that all manual annotations were performed by a single person, which might result in bias in estimating the actual ground truth annotation. Future research should minimise this bias using an average of multiple expert annotations for the same volume.

Table 4.3: Dice similarity coefficient (Dice score) comparison of our method and other literature. The mean Dice scores are displayed with either a 95% Confidence interval ([-]) or standard deviation ($\pm$). T2WI: T2-weighted MRI

Author	Method	Image modality	Spine region	Segmentation tasks		
				Spinous process	Vertebrae	External testset
Ebrahimi et al. [91]	Random Forest	X-ray	C1-C7	0.88 $\pm$ 0.08	-	-
Lu et al. [92]	U-net	Sagittal T2WI	T12-L5	-	0.93 $\pm$ 0.02	-
			S1	-	0.93 $\pm$ 0.03	-
Wang et al. [93]	U-Net	Sagittal T2WI	L1-L5	-	0.95	-
Our method	nnU-Net	Sagittal T2WI	L1-L5	0.94 [0.93 - 0.94]	-	0.93 [0.91 - 0.95]
			S1	0.87 [0.85 - 0.89]	-	0.50 [0.43 - 0.56]

4.6. Conclusions

In conclusion, the automatic annotation of MRI-based SP contours using deep learning showed a successful matching in all 16 cases. As part of our approach, we developed a segmentation algorithm that provided excellent results in an internal test set and performed well in external validation. Future research should further automate the method, evaluating the method based on entire slices and adding an object-based detector for the SP ROIs. Eventually, the approach should be integrated into the Lumbar Localiser, thereby improving the matching and user-friendliness of this ultrasound-based navigation approach.

5

General discussion and conclusions

This master's thesis aims to improve and evaluate the ultrasound-based level localisation approach for spinal surgery. Our clinical study showed that the accuracy of the improved level localisation approach as it is currently was insufficient for implementation in clinical practice. This research resulted in the improvement of the technical aspects and clinical workflow of the Lumbar Localiser. We showed that pre- and intraoperative ultrasound acquisitions could be efficiently integrated into the OR workflow, with clinically negligible time differences compared to the current approach. Intraoperative ultrasound acquisition enabled the surgeon to re-check the intended level of surgery without the attenuating subcutaneous fat layer between the SP and ultrasound transducer. Furthermore, the ease of use of the Lumbar Localiser was improved by the successful automatisation of the contour annotation on the preoperative images, showing excellent results.

Future research should aim to increase the accuracy of the Lumbar Localiser. The accuracy for level localisation should be around 100% to minimise the risk of WLS, thus preventing irreversible damage. Our main recommendation to improve this accuracy is to eliminate error-prone human interference. For example, contour-to-contour matching should be incorporated to facilitate intraoperative and prospective matching. Moreover, user-friendliness can be further improved by integrating our automated contour segmentation approach in the Lumbar Localiser. Future research on this deep learning-based approach should promote further automatisation, evaluating the method based on entire slices and adding an object-based detector for the SP ROIs.

The interviewed healthcare workers regard ultrasound-based level localisation as a promising approach to replace the C-arm. The lightweight and flexibility of the ultrasound system were frequently mentioned as the OR staff eagerly awaits the replacement of the heavy C-arm. A safer working environment is ensured for the healthcare workers, as no ionising radiation is required using the Lumbar Localiser and making lead skirts therefore no longer necessary. Moreover, patients' health is protected by ultrasound-based level localisation as they will not be exposed to X-ray radiation during surgery. In addition, we enabled the use of available preoperative MRI images for obtaining SP contouring, thereby replacing the need for preoperative X-ray images as proposed by Baka et al. [9]. Our proposal's potential advantages contribute to the Dutch government's vision for the healthcare system [1]. One of this document's themes is reducing health risks for patients and healthcare workers in medical procedures. Finally, we present a sustainable way of innovation, as a new application of an established technology is proposed, thus not requiring the manufacturing of new devices.

This research illustrates how a new application of an established technology can reduce toxic exposure in patients and healthcare workers. Further research into improving the accuracy of ultrasound-based level localisation can improve the safety of patients and healthcare workers in spinal surgery.

References

[1] Ministerie van Algemene Zaken, *Meer duurzaamheid in de zorg*, `https://www.rijksoverheid.nl/onderwerpen/duurzame-zorg/meer-duurzaamheid-in-de-zorg`, Nov. 2022.

[2] De minister voor Langdurige Zorg en Sport, Conny Helder, *Nieuwe prognose verwachte personeelstekort*, `https://open.overheid.nl/repository/ronl-a7e6f4b4-de5d-4dff-9815-6696fa895d48/1/pdf/kamerbrief-over-nieuwe-prognose-verwachte-personeelstekort.pdf`, Jan. 2022.

[3] Rijksinstituut voor Volksgezondheid en Milieu, *Blootstelling aan straling in de gezondheidszorg*, `https://www.rivm.nl/medische-stralingstoepassingen/blootstelling-aan-straling-in-gezondheidszorg`, Dec. 2021.

[4] M. G. Mody, A. Nourbakhsh, D. L. Stahl, M. Gibbs, M. Alfawareh, and K. J. Garges, "The prevalence of wrong level surgery among spine surgeons," *Spine (Phila. Pa. 1976)*, vol. 33, no. 2, pp. 194–198, Jan. 2008.

[5] R. Goodkin and L. L. Laska, "Wrong disc space level surgery: Medicolegal implications," *Surgical Neurology*, vol. 61, no. 4, pp. 323–341, 2004, ISSN: 0090-3019. DOI: `https://doi.org/10.1016/j.surneu.2003.08.022`.

[6] J. M. Ammerman and M. D. Ammerman, "Wrong-sided surgery," *J Neurosurg Spine*, vol. 9, no. 1, 105–6, author reply 106, 2008, ISSN: 1547-5654 (Print) 1547-5646. DOI: `10.3171/spi/2008/9/7/105`.

[7] R. Kraemer, A. Wild, H. Haak, J. Herdmann, R. Krauspe, and J. Kraemer, "Classification and management of early complications in open lumbar microdiscectomy," *European Spine Journal*, vol. 12, no. 3, pp. 239–246, 2003, ISSN: 0940-6719. DOI: `10.1007/s00586-002-0466-y`.

[8] A. A. Nubukpo-Guménù, F. K. K. Ségbédji, M. Rué, and J. Destandau, "Endospine surgery complications in lumbar herniated disc," *World Neurosurg.*, vol. 119, e78–e79, Nov. 2018.

[9] N. Baka, S. Leenstra, and T. van Walsum, "Random forest-based bone segmentation in ultrasound," *Ultrasound Med Biol*, vol. 43, no. 10, pp. 2426–2437, 2017, ISSN: 1879-291X (Electronic) 0301-5629 (Linking).

[10] S. Virk and S. Qureshi, "Navigation in minimally invasive spine surgery," *J Spine Surg*, vol. 5, no. Suppl 1, S25–S30, 2019, ISSN: 2414-469X (Print) 2414-4630 (Electronic) 2414-4630 (Linking).

[11] N. W. D. Thomas and J. Sinclair, "Image-guided neurosurgery: History and current clinical applications," *J Med Imaging Radiat Sci*, vol. 46, no. 3, pp. 331–342, 2015, ISSN: 1876-7982 (Electronic) 1876-7982 (Linking).

[12] S. M. Brown, *Image-guided surgery*, Web Page, 2018.

[13] L. T. Holly and K. T. Foley, "Intraoperative spinal navigation," *Spine (Phila Pa 1976)*, vol. 28, no. 15 Suppl, S54–61, 2003, ISSN: 1528-1159 (Electronic) 0362-2436 (Linking).

[14] M. Reid, "Ultrasonic visualization of a cervical cord cystic astrocytoma," *American Journal of Roentgenology*, vol. 131, no. 5, pp. 907–908, 1978, ISSN: 0361-803X. DOI: `10.2214/ajr.131.5.907`.

[15] S. D. Sun, B. K. Chang, and S. H. Moon, "Ultrasound-guided intervention in cervical spine," *jkoa*, vol. 50, no. 2, pp. 77–92, 2015, ISSN: 1226-2102. DOI: `10.4055/jkoa.2015.50.2.77`.

[16] T. M. Peters, "Image-guidance for surgical procedures," *Phys Med Biol*, vol. 51, no. 14, R505–40, 2006, ISSN: 0031-9155 (Print) 0031-9155 (Linking).

[17] J. B. A. Maintz and M. A. Viergever, "A survey of medical image registration," *Medical Image Analysis*, vol. 2, no. 1, pp. 1–36, 1998, ISSN: 1361-8415. DOI: `https://doi.org/10.1016/S1361-8415(01)80026-8`.

[18] M. Makuuchi, G. Torzilli, and J. Machi, "History of intraoperative ultrasound," *Ultrasound in Medicine and Biology*, vol. 24, no. 9, pp. 1229–1242, 1998, ISSN: 0301-5629. DOI: `10.1016/s0301-5629(98)00112-4`.

[19] J. H. Cook and B. Lytton, "Intraoperative localization of renal calculi during nephrolithotomy by ultrasound scanning," *J Urol*, vol. 117, no. 5, pp. 543–6, 1977, ISSN: 0022-5347 (Print) 0022-5347. DOI: `10.1016/s0022-5347(17)58530-4`.

[20] A. Shkolnik and D. G. McLone, "Intraoperative real-time ultrasonic guidance of ventricular shunt placement in infants," *Radiology*, vol. 141, no. 2, pp. 515–7, 1981, ISSN: 0033-8419 (Print) 0033-8419. DOI: `10.1148/radiology.141.2.7291582`.

[21] G. J. Dohrmann and J. M. Rubin, "Use of ultrasound in neurosurgical operations: A preliminary report," *Surgical Neurology*, vol. 16, no. 5, pp. 362–366, 1981, ISSN: 0090-3019. DOI: `https://doi.org/10.1016/0090-3019(81)90279-2`.

[22] G. R. Giammalva, G. Ferini, S. Musso, *et al.*, "Intraoperative ultrasound: Emerging technology and novel applications in brain tumor surgery," *Frontiers in oncology*, vol. 12, pp. 818 446–818 446, 2022, ISSN: 2234-943X. DOI: `10.3389/fonc.2022.818446`.

[23] M. Ganau, N. Syrmos, A. R. Martin, F. Jiang, and M. G. Fehlings, "Intraoperative ultrasound in spine surgery: History, current applications, future developments," *Quantitative Imaging in Medicine and Surgery*, vol. 8, no. 3, pp. 261–267, 2018, ISSN: 2223-4292. DOI: `10.21037/qims.2018.04.02`.

[24] F. Prada, M. D. Bene, R. Fornaro, *et al.*, "Identification of residual tumor with intraoperative contrast-enhanced ultrasound during glioblastoma resection," *Neurosurg Focus*, vol. 40, no. 3, E7, 2016, ISSN: 1092-0684. DOI: `10.3171/2015.11.Focus15573`.

[25] K. Mursch, M. Scholz, W. Brück, and J. Behnke-Mursch, "The value of intraoperative ultrasonography during the resection of relapsed irradiated malignant gliomas in the brain," *Ultrasonography*, vol. 36, no. 1, pp. 60–65, 2017, ISSN: 2288-5919 (Print) 2288-5919. DOI: `10.14366/usg.16015`.

[26] O. M. Rygh, T. Selbekk, S. H. Torp, S. Lydersen, T. A. Hernes, and G. Unsgaard, "Comparison of navigated 3d ultrasound findings with histopathology in subsequent phases of glioblastoma resection," *Acta Neurochir (Wien)*, vol. 150, no. 10, 1033–41, discussion 1042, 2008, ISSN: 0001-6268. DOI: `10.1007/s00701-008-0017-3`.

[27] J. Coburger, A. Scheuerle, D. R. Thal, *et al.*, "Linear array ultrasound in low-grade glioma surgery: Histology-based assessment of accuracy in comparison to conventional intraoperative ultrasound and intraoperative mri," *Acta Neurochir (Wien)*, vol. 157, no. 2, pp. 195–206, 2015, ISSN: 0001-6268. DOI: `10.1007/s00701-014-2314-3`.

[28] L. G. Cheng, W. He, H. X. Zhang, *et al.*, "Intraoperative contrast enhanced ultrasound evaluates the grade of glioma," *Biomed Res Int*, vol. 2016, p. 2 643 862, 2016, ISSN: 2314-6133 (Print). DOI: `10.1155/2016/2643862`.

[29] M. Tiouririne, A. J. Dixon, F. W. Mauldin, D. Scalzo, and A. Krishnaraj, "Imaging performance of a handheld ultrasound system with real-time computer-aided detection of lumbar spine anatomy," *Investigative Radiology*, vol. 52, no. 8, pp. 447–455, 2017, ISSN: 1536-0210. DOI: `10.1097/rli.0000000000000361`.

[30] F. Yan, Z. Song, M. Du, and A. L. Klibanov, "Ultrasound molecular imaging for differentiation of benign and malignant tumors in patients," *Quant Imaging Med Surg*, vol. 8, no. 11, pp. 1078–1083, 2018, ISSN: 2223-4292 (Print) 2223-4306. DOI: `10.21037/qims.2018.12.08`.

[31] M. A. Pino, A. Imperato, I. Musca, *et al.*, "New hope in brain glioma surgery: The role of intraoperative ultrasound. a review," *Brain sciences*, vol. 8, no. 11, p. 202, 2018, ISSN: 2076-3425. DOI: `10.3390/brainsci8110202`.

[32] B. Saß, M. Bopp, C. Nimsky, and B. Carl, "Navigated 3-dimensional intraoperative ultrasound for spine surgery," *World Neurosurgery*, vol. 131, e155–e169, 2019, ISSN: 1878-8750. DOI: `10.1016/j.wneu.2019.07.188`.

[33] A. Patel and et al., "A reproducible and reliable localization technique for lumbar spine surgery that minimizes unintended-level exposure and wrong-level surgery," *Spine Journal, The*, vol. 19, no. 5, p. 773, 2019, ISSN: 1529-9430.

[34] J. Tat, J. Tat, S. Yoon, A. J. M. Yee, and J. Larouche, "Intraoperative ultrasound in spine decompression surgery: A systematic review," *Spine (Phila Pa 1976)*, vol. 47, no. 2, E73–E85, 2022, ISSN: 1528-1159 (Electronic) 0362-2436 (Linking).

[35] E. Watanabe, T. Watanabe, S. Manaka, Y. Mayanagi, and K. Takakura, "Three-dimensional digitizer (neuronavigator): New equipment for computed tomography-guided stereotaxic surgery," *Surgical Neurology*, vol. 27, no. 6, pp. 543–547, 1987, ISSN: 0090-3019. DOI: https://doi.org/10.1016/0090-3019(87)90152-2.

[36] R. Galloway and T. Peters, "Overview and history of image-guided interventions," in *Image-Guided Interventions: Technology and Applications*, T. Peters and K. Cleary, Eds. Boston, MA: Springer US, 2008, pp. 1–21, ISBN: 978-0-387-73858-1. DOI: 10.1007/978-0-387-73858-1_1.

[37] Washington University School of Medicine in St. Louis, *Stereotactic neurosurgical procedures*, https://neurosurgery.wustl.edu/items/stereotactic-neurosurgical-procedures.

[38] V. Horsley and R. H. Clarke, "The structure and functions of the cerebellum examined by a new method," *Brain*, vol. 31, no. 1, pp. 45–124, 1908, ISSN: 0006-8950. DOI: 10.1093/brain/31.1.45.

[39] E. A. Spiegel, H. T. Wycis, M. Marks, and A. J. Lee, "Stereotaxic apparatus for operations on the human brain," *Science*, vol. 106, no. 2754, pp. 349–350, 1947. DOI: 10.1126/science.106.2754.349.

[40] C. R. Wirtz, M. M. Bonsanto, M. Knauth, *et al.*, "Intraoperative magnetic resonance imaging to update interactive navigation in neurosurgery: Method and preliminary experience," *Computer Aided Surgery*, vol. 2, no. 3-4, pp. 172–179, 1997, ISSN: 1092-9088. DOI: 10.3109/10929089709148110.

[41] R. Comeau, A. Fenster, and T. Peters, *Integrated MR and ultrasound imaging for improved image guidance in neurosurgery* (Medical Imaging '98). SPIE, 1998, vol. 3338.

[42] P. A. Helm, R. Teichman, S. L. Hartmann, and D. Simon, "Spinal navigation and imaging: History, trends, and future," *IEEE Transactions on Medical Imaging*, vol. 34, no. 8, pp. 1738–1746, 2015, ISSN: 0278-0062. DOI: 10.1109/tmi.2015.2391200.

[43] J. W. Trobaugh, W. D. Richard, K. R. Smith, and R. D. Bucholz, "Frameless stereotactic ultrasonography: Method and applications," *Comput Med Imaging Graph*, vol. 18, no. 4, pp. 235–46, 1994, ISSN: 0895-6111 (Print) 0895-6111. DOI: 10.1016/0895-6111(94)90048-5.

[44] S. Ohue, Y. Kumon, S. Nagato, *et al.*, "Evaluation of intraoperative brain shift using an ultrasound-linked navigation system for brain tumor surgery," *Neurologia medico-chirurgica*, vol. 50, no. 4, pp. 291–300, 2010, ISSN: 0470-8105. DOI: 10.2176/nmc.50.291.

[45] D. f. Wu, W. He, S. Lin, C.-S. Zee, and B. Han, "The real-time ultrasonography for fusion image in glioma neurosugery," *Clinical Neurology and Neurosurgery*, vol. 175, pp. 84–90, 2018, ISSN: 0303-8467. DOI: https://doi.org/10.1016/j.clineuro.2018.10.009.

[46] F. Prada, M. Del Bene, L. Mattei, *et al.*, "Preoperative magnetic resonance and intraoperative ultrasound fusion imaging for real-time neuronavigation in brain tumor surgery," *Ultraschall in der Medizin - European Journal of Ultrasound*, vol. 36, no. 02, pp. 174–186, 2014, ISSN: 0172-4614. DOI: 10.1055/s-0034-1385347.

[47] J. Nitsch, J. Klein, P. Dammann, *et al.*, "Automatic and efficient mri-us segmentations for improving intraoperative image fusion in image-guided neurosurgery," *Neuroimage Clin*, vol. 22, p. 101 766, 2019, ISSN: 2213-1582. DOI: 10.1016/j.nicl.2019.101766.

[48] I. A. Rasmussen, F. Lindseth, O. M. Rygh, *et al.*, "Functional neuronavigation combined with intraoperative 3d ultrasound: Initial experiences during surgical resections close to eloquent brain areas and future directions in automatic brain shift compensation of preoperative data," *Acta Neurochirurgica*, vol. 149, no. 4, pp. 365–378, 2007, ISSN: 0001-6268. DOI: 10.1007/s00701-006-1110-0.

[49] S. Hu, H. Kang, Y. Baek, G. Fakhri, A. Kuang, and H. Choi, "Real-time imaging of brain tumor for image-guided surgery," *Advanced Healthcare Materials*, vol. 7, p. 1 800 066, 2018. DOI: 10.1002/adhm.201800066.

[50] T. De Silva, A. Uneri, X. Zhang, *et al.*, "Real-time, image-based slice-to-volume registration for ultrasound-guided spinal intervention," *Physics in Medicine and Biology*, vol. 63, no. 21, p. 215 016, 2018, ISSN: 1361-6560. DOI: `10.1088/1361-6560/aae761`.

[51] B. Fuerst, W. Wein, M. Müller, and N. Navab, "Automatic ultrasound–mri registration for neurosurgery using the 2d and 3d lc2 metric," *Medical Image Analysis*, vol. 18, no. 8, pp. 1312–1319, 2014, ISSN: 1361-8415. DOI: `https://doi.org/10.1016/j.media.2014.04.008`.

[52] H. E. Gueziri, C. Santaguida, and D. L. Collins, "The state-of-the-art in ultrasound-guided spine interventions," *Medical Image Analysis*, vol. 65, p. 101 769, 2020, ISSN: 1361-8415. DOI: `10.1016/j.media.2020.101769`.

[53] A. Lang, P. Mousavi, S. Gill, G. Fichtinger, and P. Abolmaesumi, "Multi-modal registration of speckle-tracked freehand 3d ultrasound to ct in the lumbar spine," *Medical Image Analysis*, vol. 16, no. 3, pp. 675–686, 2012, ISSN: 1361-8415. DOI: `https://doi.org/10.1016/j.media.2011.07.006`.

[54] H. E. Gueziri, S. Drouin, C. X. B. Yan, and D. L. Collins, "Toward real-time rigid registration of intraoperative ultrasound with preoperative ct images for lumbar spinal fusion surgery," *International Journal of Computer Assisted Radiology and Surgery*, vol. 14, no. 11, pp. 1933–1943, 2019, ISSN: 1861-6410. DOI: `10.1007/s11548-019-02020-1`.

[55] S. Nagpal, P. Abolmaesumi, A. Rasoulian, *et al.*, "A multi-vertebrae ct to us registration of the lumbar spine in clinical data," *Int J Comput Assist Radiol Surg*, vol. 10, no. 9, pp. 1371–81, 2015, ISSN: 1861-6429 (Electronic) 1861-6410 (Linking).

[56] F. Chen, D. Wu, and H. Liao, "Registration of ct and ultrasound images of the spine with neural network and orientation code mutual information," in Springer International Publishing, 2016, pp. 292–301, ISBN: 0302-9743. DOI: `10.1007/978-3-319-43775-0_26`.

[57] G. M. Malham and T. Wells-Quinn, "What should my hospital buy next?-guidelines for the acquisition and application of imaging, navigation, and robotics for spine surgery," *Journal of spine surgery (Hong Kong)*, vol. 5, no. 1, pp. 155–165, 2019, ISSN: 2414-469X 2414-4630. DOI: `10.21037/jss.2019.02.04`.

[58] Bimedis, *Philips sparq*, `https://bimedis.com/philips-sparq-m2752`, Web Page, 2022.

[59] Y. Liu, M. G. Lee, and J. S. Kim, "Spine surgery assisted by augmented reality: Where have we been?" *Yonsei Med J*, vol. 63, no. 4, pp. 305–316, 2022, ISSN: 0513-5796 (Print) 0513-5796. DOI: `10.3349/ymj.2022.63.4.305`.

[60] H. Verbiest, "Primary stenosis of the lumbar spinal canal in adults, a new syndrome.," *Ned Tijdschr Geneeskd*, vol. 94, pp. 2415–2433, 1950.

[61] H. Verbiest, "A radicular syndrome from developmental narrowing of the lumbar vertebral canal," *J. Bone Joint Surg. Br.*, vol. 36-B, no. 2, pp. 230–237, May 1954.

[62] J. Deasy, "Acquired lumbar spinal stenosis," *Jaapa*, vol. 28, no. 4, pp. 19–23, 2015, ISSN: 1547-1896 (Print) 0893-7400. DOI: `10.1097/01.JAA.0000462052.47882.fd`.

[63] A. M. Wu, F. Zou, Y. Cao, *et al.*, "Lumbar spinal stenosis: An update on the epidemiology, diagnosis and treatment," *AME Medical Journal*, vol. 2, no. 5, 2017, ISSN: 2520-0518.

[64] R. A. Deyo, D. T. Gray, W. Kreuter, S. Mirza, and B. I. Martin, "United states trends in lumbar fusion surgery for degenerative conditions," *Spine (Phila. Pa. 1976)*, vol. 30, no. 12, 1441–5, discussion 1446–7, Jun. 2005.

[65] J. Jordan, K. Konstantinou, and J. O'Dowd, "Herniated lumbar disc," *BMJ Clin. Evid.*, vol. 2011, Jun. 2011.

[66] G. Cooper, "Clinical anatomy of the lumbosacral spine," in *Non-Operative Treatment of the Lumbar Spine*. Cham: Springer International Publishing, 2015, pp. 3–10, ISBN: 978-3-319-21443-6. DOI: `10.1007/978-3-319-21443-6_1`.

[67] Mayo Foundation for Medical Education and Research, *Laminectomy*, `https://www.mayoclinic.org/tests-procedures/laminectomy/about/pac-20394533#dialogId5883849`, Jun. 2022.

[68] Mayo Foundation for Medical Education and Research, *Diskectomy*, `https://www.mayoclinic.org/tests-procedures/diskectomy/about/pac-20393837`, Jul. 2022.

[69] O. Merz, U. Wolf, M. Robert, V. Gesing, and M. Rominger, "Validity of palpation techniques for the identification of the spinous process L5," *Man. Ther.*, vol. 18, no. 4, pp. 333–338, Aug. 2013.

[70] C. R. Broadbent, W. B. Maxwell, R. Ferrie, D. J. Wilson, M. Gawne-Cain, and R. Russell, "Ability of anaesthetists to identify a marked lumbar interspace," *Anaesthesia*, vol. 55, no. 11, pp. 1122–1126, Nov. 2000.

[71] K. T. Snider, J. W. Kribs, E. J. Snider, B. F. Degenhardt, A. Bukowski, and J. C. Johnson, "Reliability of tuffier's line as an anatomic landmark," *Spine (Phila. Pa. 1976)*, vol. 33, no. 6, E161–5, Mar. 2008.

[72] R. Chakraverty, P. Pynsent, and K. Isaacs, "Which spinal levels are identified by palpation of the iliac crests and the posterior superior iliac spines?" *J. Anat.*, vol. 210, no. 2, pp. 232–236, Feb. 2007.

[73] C. B. Margarido, R. Mikhael, C. Arzola, M. Balki, and J. C. A. Carvalho, "The intercristal line determined by palpation is not a reliable anatomical landmark for neuraxial anesthesia," *Can. J. Anaesth.*, vol. 58, no. 3, pp. 262–266, Mar. 2011.

[74] A. Z. Naqvi, H. Magill, and N. Anjarwalla, "Intraoperative practices to prevent wrong-level spine surgery: A survey among 105 spine surgeons in the united kingdom," *Patient Saf. Surg.*, vol. 16, no. 1, p. 6, Jan. 2022.

[75] J. E. Mayer, R. P. Dang, G. F. Duarte Prieto, S. K. Cho, S. A. Qureshi, and A. C. Hecht, "Analysis of the techniques for thoracic- and lumbar-level localization during posterior spine surgery and the occurrence of wrong-level surgery: Results from a national survey," *Spine J.*, vol. 14, no. 5, pp. 741–748, May 2014.

[76] M. Shah, D. R. Halalmeh, A. Sandio, R. S. Tubbs, and M. D. Moisi, "Anatomical variations that can lead to spine surgery at the wrong level: Part III lumbosacral spine," *Cureus*, vol. 12, no. 7, e9433, Jul. 2020.

[77] Philips, *Iu22 xmatrix ultrasound system*, `https://www.philips.nl/healthcare/product/HC795050/iu22-xmatrix-ultrasound-system`. (visited on 10/09/2022).

[78] Philips, *Sparq ultrasound system*, `https://www.philips.nl/healthcare/product/HC795090RA/sparq-ultrasound-system`. (visited on 10/09/2022).

[79] Epiphan, *Av.io hd - usb video grabber for hdmi video capture*, `https://www.epiphan.com/products/avio-hd/`, May 2022.

[80] K. Simfukwe, I. Iakimov, R. Sufianov, L. Borba, L. Mastronardi, and A. Shumadalova, "Application of intraoperative ultrasound navigation in neurosurgery," *Front. Surg.*, vol. 9, p. 900 986, May 2022.

[81] H. E. Gueziri, O. Rabau, C. Santaguida, and D. L. Collins, "Evaluation of an ultrasound-based navigation system for spine neurosurgery: A porcine cadaver study," *Frontiers in Oncology*, vol. 11, 2021, ISSN: 2234-943X.

[82] R. Prevost, M. Salehi, S. Jagoda, *et al.*, "3d freehand ultrasound without external tracking using deep learning," *Medical Image Analysis*, vol. 48, pp. 187–202, 2018, ISSN: 1361-8415. DOI: `https://doi.org/10.1016/j.media.2018.06.003`.

[83] K. S. Talekar, E. Smith, and A. E. Flanders, "Imaging spinal stenosis," *Applied Radiology*, vol. 46, no. 1, pp. 8–17, Jan. 2017.

[84] F. Isensee, P. F. Jaeger, S. A. A. Kohl, J. Petersen, and K. H. Maier-Hein, "nnU-Net: A self-configuring method for deep learning-based biomedical image segmentation," *Nat. Methods*, vol. 18, no. 2, pp. 203–211, Feb. 2021.

[85] F. Isensee, J. Petersen, S. A. A. Kohl, P. F. Jäger, and K. H. Maier-Hein, "Nnu-net: Breaking the spell on successful medical image segmentation," *CoRR*, vol. abs/1904.08128, 2019. arXiv: `1904.08128`.

[86] M. Antonelli, A. Reinke, S. Bakas, *et al.*, "The medical segmentation decathlon," *Nat. Commun.*, vol. 13, no. 1, p. 4128, Jul. 2022.

[87] O. Ronneberger, P. Fischer, and T. Brox, "U-net: Convolutional networks for biomedical image segmentation," N. Navab, J. Hornegger, W. M. Wells, and A. F. Frangi, Eds., pp. 234–241, 2015.

[88] F. Isensee, *Function convert 2d image to nifti*, `https://github.com/MIC-DKFZ/nnUNet/blob/aa53b3b87130ad78f0a28e6169a83215d708d659/nnunet/utilities/file_conversions.py#L8`, Apr. 2021.

[89] SciPy, *Scipy.ndimage.measurements.label*, `https://docs.scipy.org/doc/scipy-0.14.0/reference/generated/scipy.ndimage.measurements.label.html`, May 2014.

[90] HiLab-git, *Python get largest component*, `https://www.programcreek.com/python/?CodeExample=get%2Blargest%2Bcomponent`.

[91] S. Ebrahimi, L. Gajny, W. Skalli, and E. D. Angelini, "Automatic segmentation and identification of spinous processes on sagittal x-rays based on random forest classification and dedicated contextual features," in *2019 IEEE 16th International Symposium on Biomedical Imaging (ISBI 2019)*, 2019, pp. 688–691. DOI: `10.1109/ISBI.2019.8759490`.

[92] J. T. Lu, S. Pedemonte, B. C. Bizzo, *et al.*, "Deep spine: Automated lumbar vertebral segmentation, disc-level designation, and spinal stenosis grading using deep learning," in *Machine Learning in Health Care*, 2018.

[93] S. Wang, Z. Jiang, H. Yang, X. Li, and Z. Yang, "Automatic segmentation of lumbar spine MRI images based on improved attention U-Net," *Comput. Intell. Neurosci.*, vol. 2022, p. 4 259 471, Sep. 2022.